AMERICAN SOCIETY FOR MICROBIOLOGY | Molecular and Cellular Biology®

RESEARCH ARTICLE

Targeting Protein Tyrosine Phosphatase 22 Does Not Enhance the Efficacy of Chimeric Antigen Receptor T Cells in Solid Tumors

Xin Du,[a,d] Phillip K. Darcy,[a,d] Florian Wiede,[a,b,c] Tony Tiganis[a,b,c]

[a]Peter MacCallum Cancer Centre, Melbourne, Victoria, Australia
[b]Monash Biomedicine Discovery Institute, Monash University, Clayton, Victoria, Australia
[c]Department of Biochemistry and Molecular Biology, Monash University, Clayton, Victoria, Australia
[d]Sir Peter MacCallum Department of Oncology, University of Melbourne, Parkville, Victoria, Australia

SUMMARY Adoptive cell therapy with chimeric antigen receptor (CAR) T cells has revolutionized the treatment of certain B cell malignancies but has been in ineffective against solid tumors. Recent studies have highlighted the potential of targeting negative regulators of T cell signaling to enhance the efficacy and extend the utility of CAR T cells to solid tumors. Autoimmunity-linked protein tyrosine phosphatase N22 (PTPN22) has been proposed as a target for cancer immunotherapy. Here, we have used CRISPR/Cas9 gene editing to generate PTPN22-deficient (*Ptpn22*$^{\Delta/\Delta}$) mice (C57BL/6) and assessed the impact of PTPN22 deficiency on the cytotoxicity and efficacy of CAR T cells *in vitro* and *in vivo*. As reported previously, PTPN22 deficiency was accompanied by the promotion of effector T cell responses *ex vivo* and the repression of syngeneic tumor growth *in vivo*. However, PTPN22 deficiency did not enhance the cytotoxic activity of murine CAR T cells targeting the extracellular domain of the human oncoprotein HER2 *in vitro*. Moreover, PTPN22-deficient α-HER2 CAR T cells or ovalbumin-specific OT-I CD8$^+$ T cells adoptively transferred into mice bearing HER2$^+$ mammary tumors or ovalbumin-expressing mammary or colorectal tumors, respectively, were no more effective than their wild-type counterparts in suppressing tumor growth. The deletion of PTPN22 using CRISPR/Cas9 gene editing also did not affect the cytotoxic activity of human CAR T cells targeting the Lewis Y antigen that is expressed by many human solid tumors. Therefore, PTPN22 deficiency does not enhance the antitumor activity of CAR T cells in solid organ malignancies.

KEYWORDS CAR T cell, PTPN22, protein tyrosine phosphatase, T cell, immunotherapy, tumor, tumor immunology

Therapies that enhance the immune response to tumors have revolutionized the management of cancer. However, most tumors do not have a high mutational burden and are therefore not seen by the immune system or otherwise evolve mechanisms to escape immune surveillance (1–4). Therefore, such tumors remain unresponsive to class-leading immunotherapies, including those targeting immune checkpoints (3, 4). Chimeric antigen receptor (CAR) T cell therapy has the potential to overcome such limitations, as it is not reliant on endogenous antitumor immunity (5–7).

CAR T cell therapy involves the adoptive transfer of autologous T cells engineered to express an extracellular short-chain variable fragment targeting a defined tumor antigen, and an intracellular signaling domain that typically comprises components of the T cell receptor (TCR) such as CD3ζ and costimulatory receptors such as CD28 (5–7). When CARs engage their target antigen, they are thought to signal via canonical TCR and coreceptor signaling intermediates, including via the Src family kinase (SFK) LCK, to promote CAR T cell expansion, activation, and cytotoxicity (8, 9). CAR T cells targeting CD19 are Food and

Address correspondence to Florian Wiede, Florian.Wiede@monash.edu, or Tony Tiganis, Tony.Tiganis@monash.edu.

The authors declare a conflict of interest. F.W. and T.T. have patent applications on targeting PTPN2 in cancer immunotherapy held by Monash University. T.T. is on the Scientific Advisory Board and receives research funding from DepYmed.

Received 17 September 2021
Returned for modification 12 November 2021
Accepted 27 December 2021
Accepted manuscript posted online 18 January 2022
Published 17 March 2022

Drug Administration (FDA)-approved for the treatment of relapsed B-cell acute lymphoblastic leukemia (ALL) and aggressive non-Hodgkin's lymphoma (6, 10). Indeed, CD19 CAR T cells have resulted in remarkable efficacy in B cell ALL with clinical response rates of up to 90% (5, 9–11). However, there are numerous limitations that prohibit the widespread use of CAR T cells (5–7). In particular, CAR T cells need to home to and infiltrate solid tumors and thereon overcome immunosuppression and exhaustion within the tumor microenvironment (5–7). Our recent studies have shown that such challenges can be overcome by targeting protein tyrosine phosphatases (PTPs) that attenuate TCR/CAR and/or cytokine signaling (12). In particular, we have shown that the deletion of the tyrosine-specific phosphatase PTPN2 (also known as TCPTP) and the promotion of both LCK and cytokine-induced Janus-activated kinase (JAK)/signal transducer and activator of transcription 5 (STAT5) signaling promotes both CAR T cell homing/infiltration and activation to eradicate mammary tumors in mice (12). As with the T cell inhibitory receptor PD-1, which normally functions to maintain T cell tolerance and prevent autoimmunity (13–15), PTPN2 is instrumental in the maintenance of T cell tolerance and its deletion in T cells or the hematopoietic compartment can promote systemic inflammation and autoimmunity (16–18). Indeed, loss-of-function *PTPN2* single-nucleotide polymorphisms (SNPs) have been linked with autoimmune diseases, including type 1 diabetes, rheumatoid arthritis, and Crohn's disease in humans (19, 20). Accordingly, we reasoned that other PTPs implicated in T cell tolerance might also serve as effective targets for enhancing the efficacy of CAR T cells.

PTPN22 (also known as LYP in humans or PEP in mice) is also a classical tyrosine-specific phosphatase that is expressed abundantly in hematopoietic cells (21, 22). PTPN22 has distinct roles in cells of the innate and adaptive immune compartments (21, 22). In T cells, PTPN22 dephosphorylates several protein tyrosine kinases (PTKs) and tyrosine phosphorylated substrates, including CD3ε, LCK, and the Syk family tyrosine kinase ZAP-70 to attenuate TCR signaling (23). However, the effects of PTPN22 on TCR signaling appear to be restricted to the effector and memory T cell subsets, where PTPN22 expression is more abundant (23). The global deletion of PTPN22 (*Ptpn22*$^{-/-}$) in aged C57BL/6 mice results in the accumulation of effector T cells that are more responsive to TCR ligation (23). Moreover, aged *Ptpn22*$^{-/-}$ C57BL/6 mice have increased CD4$^+$ follicular helper T cells and form spontaneous germinal centers in the spleen (23). However, PTPN22 deletion also increases CD4$^+$ CD25$^+$ FoxP3$^+$ regulatory T cells (T_{regs}) and enhances their capacity to suppress CD8$^+$ T cell function (24, 25). Beyond its role in T cells, PTPN22 also exerts effects on innate immunity, where it can elicit inhibitory and stimulatory functions, attenuating interferon (IFN)-α receptor signaling (26), while promoting the release of myeloid-derived type 1 IFNs by dephosphorylating NRLP3 to regulate inflammasome activation (27) and by nonenzymatically regulating TRAF3 ubiquitination and degradation (26). Notably, the *PTPN22*(*C1858T*) polymorphism results in a missense R620W mutation and has been linked with the development of systemic lupus erythematosus, type 1 diabetes, rheumatoid arthritis, and other autoimmune disorders (21, 22). Moreover, as for PTPN2 (12), the deletion of PTPN22 in mice has been reported to enhance antitumor immunity (28), as well as the ability of adoptively transferred T cells to repress the growth of tumors bearing low, but not high-affinity antigens (29, 30). Therefore, in this study, we explored whether targeting PTPN22 might also enhance the efficacy of CAR T cells.

RESULTS

Generation and characterization of PTPN22-deficient mice. To assess the impact of deleting PTPN22 on antitumor immunity and CAR T cell therapy, we used CRISPR/Cas9 genome editing (31) to produce C57BL/6 mice with a global deficiency in *PTPN22* (Fig. 1). These mice arose by nonhomologous end joining in the course of generating PTPN22 R619W mutant mice; an adenine insertion was introduced between nucleotides 1854 and 1855 resulting in a R619T substitution, followed by a 24-nucleotide insertion and a stop codon to produce a truncated 628-amino-acid protein (as opposed to 802 amino acids for full-length PTPN22) with a predicted molecular weight of 69 kDa (Fig. 1A). The frameshift and premature stop codon resulted in mRNA (as assessed by real-time PCR) that was reduced by $>$ 70% in lymphoid cells and a truncated protein whose relative abundance was reduced

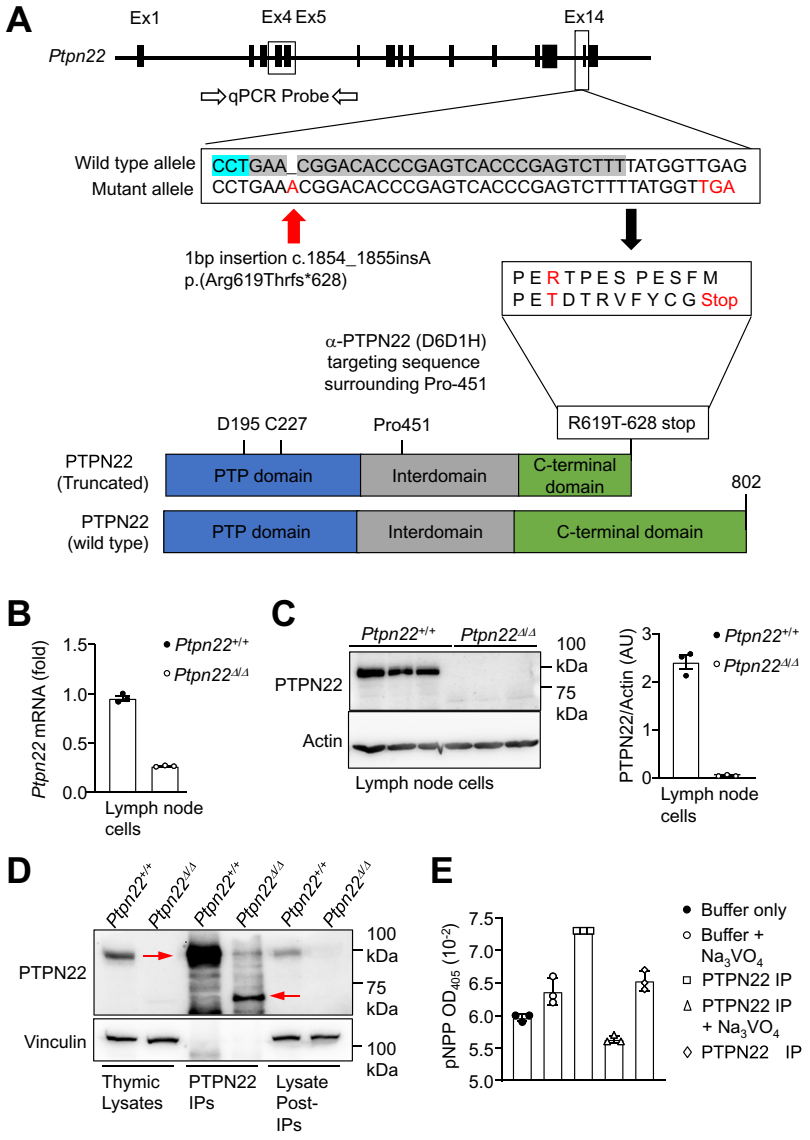

FIG 1 Generation of *Ptpn22*$^{\Delta/\Delta}$ mice. (A) *Ptpn22*$^{\Delta/\Delta}$ mutant mice were generated on a C57BL/6 background using CRISPR/Cas9 genome editing. These mice arose by nonhomologous end-joining in the course of generating PTPN22 R619W mutant mice; an adenine insertion was introduced between nucleotides 1854 and 1855 resulting in a R619T substitution, followed by a 24-nucleotide insertion and a TGA stop codon to produce a truncated 628-amino-acid protein. Real-time PCR probes targeting the boundaries of exons 4 and 5 were used to quantify *Ptpn22* mRNA levels, and a rabbit monoclonal PTPN22 antibody (D6D1H) specific for the sequence surrounding Pro-451 in the PTPN22 interdomain region was used to detect PTPN22 by immunoblotting. (B) *Ptpn22* mRNA levels in lymph node cells from *Ptpn22*$^{+/+}$ and *Ptpn22*$^{\Delta/\Delta}$ C57BL/6 mice analyzed by quantitative real-time PCR. (C) PTPN22 and mutant PTPN22 (PTPN22Δ) protein in lymph node cells from *Ptpn22*$^{+/+}$ and *Ptpn22*$^{\Delta/\Delta}$ C57BL/6 mice analyzed by immunoblotting with PTPN22 antibody (D6D1H). (D) α-PTPN22 (D6D1H) was used to immunoprecipitate (IP) PTPN22 or PTPN22Δ from the thymic lysates of *Ptpn22*$^{+/+}$ and *Ptpn22*$^{\Delta/\Delta}$ mice and IPs processed for immunoblotting. (E) PTP activity in PTPN22 and PTPN22Δ IPs from the thymic lysates of *Ptpn22*$^{+/+}$ and *Ptpn22*$^{\Delta/\Delta}$ mice was assessed using *p*-nitrophenyl phosphate (pNPP) as a substrate in the presence or absence of 1 mM Na_3VO_4 as indicated.

by >95%, consistent with the introduced mutation resulting in both mRNA and protein instability (Fig. 1B and C). The truncation was not associated with any overt increase in phosphatase activity, as assessed in PTPN22 immunoprecipitates using *p*-nitrophenol phosphate as a substrate (Fig. 1D and E). These results are consistent with the introduced mutation generating a hypomorph that will hereon be referred to as *Ptpn22*$^{\Delta/\Delta}$ (encoding PTPN22Δ). Given the significant reduction in PTPN22Δ protein, we determined the extent to which *Ptpn22*$^{\Delta/\Delta}$ (C57BL/6) mice resemble *Ptpn22*$^{-/-}$ (C57BL/6) mice (23) that are null for PTPN22.

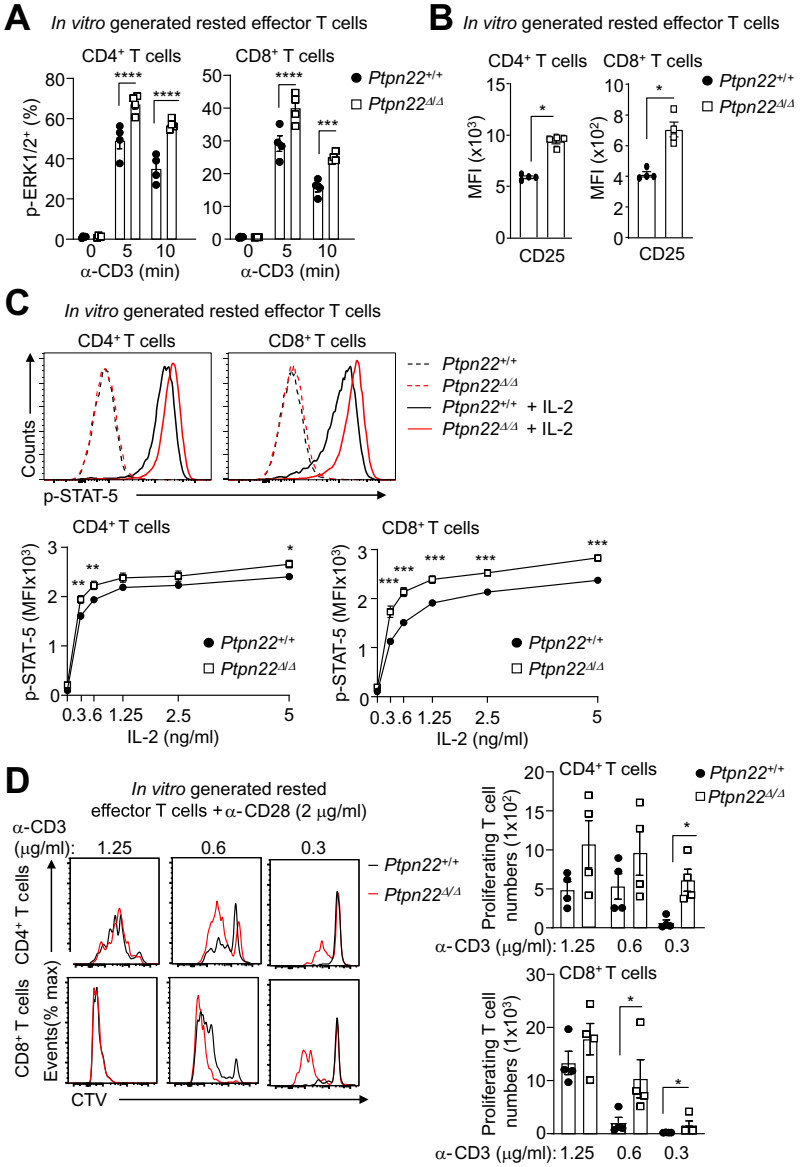

FIG 2 PTPN22 deficiency enhances TCR and IL-2 signaling in *in vitro* generated effector T cells. LN T cells form *Ptpn22*$^{+/+}$ and *Ptpn22*$^{\Delta/\Delta}$ mice were stimulated with α-CD3ε (0.5 μg/mL) and α-CD28 (0.5 μg/mL) for 48 h and then rested in T cell media supplemented with IL-7 (0.2 ng/mL) and IL-15 (10 ng/mL) for 72 h to generate rested effector T cells. (A) T cells were left untreated or stimulated with α-CD3 (5 μg/mL) and α-hamster IgG (20 μg/mL) for the indicated times and phosphorylated ERK1/2 (p-ERK1/2) positive T cells analyzed by flow cytometry. (B) CD25 (IL2Rα) cytokine receptor levels were determined by flow cytometry. (C) T cells were stimulated with the indicated concentrations of IL-2 for 20 min, and intracellular STAT-5 Y694 phosphorylation (p-STAT-5) was assessed by flow cytometry. (D) CTV-labeled rested effector T cells were stimulated with the indicated concentrations of plate-bound α-CD3ε plus α-CD28 (2 μg/mL) for 3 days, and CTV dilution was assessed by flow cytometry. Representative results (means $\pm$ the SEM) from at least two independent experiments are shown. Significance in panel A was determined using one-way ANOVA, in panels B and D using a two-tailed Mann-Whitney U test, and in panel C using two-way ANOVA (*, $P < 0.05$; **, $P < 0.01$; ***, $P < 0.001$; ****, $P < 0.0001$).

Aged (8-month-old) *Ptpn22*$^{\Delta/\Delta}$ mice exhibited splenomegaly associated with increased total cellularity, including increased T cell, B cell, and myeloid cellularity, as reported previously for *Ptpn22*$^{-/-}$ mice (23) (see Fig. S1a to d; gating strategy, Fig. S2a and b). Also, lymphoid and nonlymphoid CD4$^+$ and CD8$^+$ T cells had a predominant CD44^{hi}CD62^{lo} effector/memory or CD44^{hi}CD62^{hi} central memory phenotype, splenic and lymph node CD25$^+$FoxP3$^+$ T$_{regs}$ were more abundant (see Fig. S3a and b and Fig. S1b and c), and PNA$^+$ germinal centers were

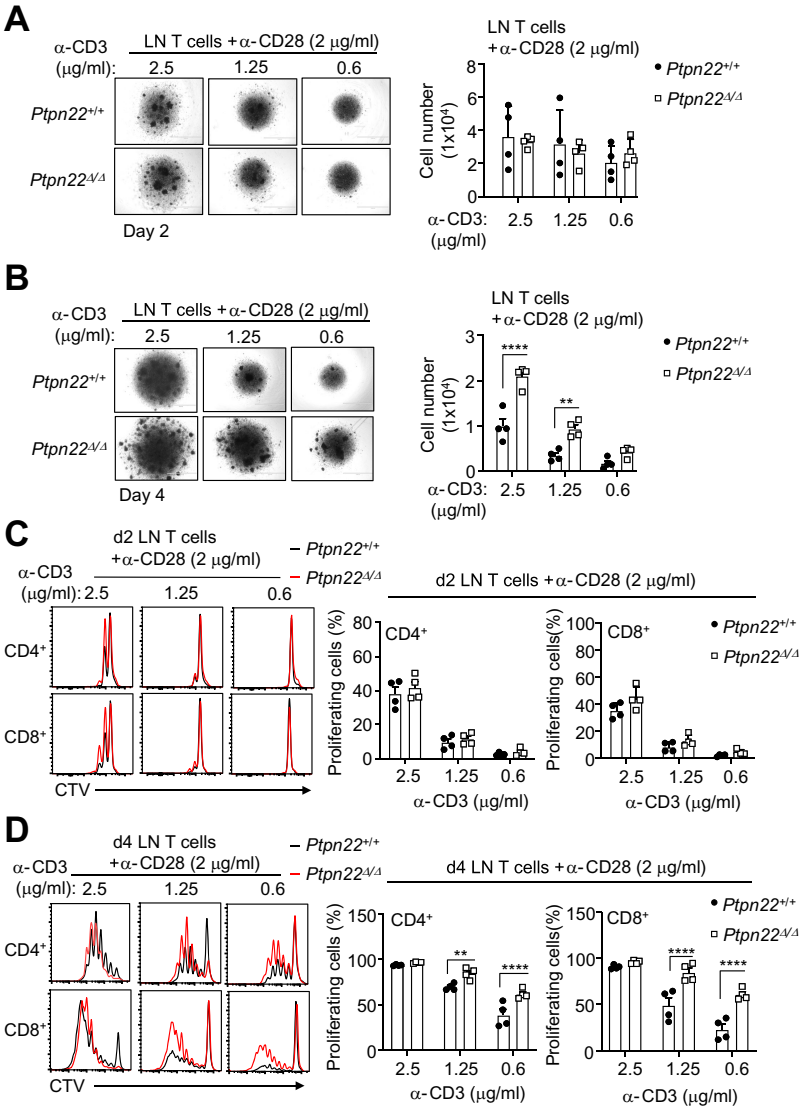

FIG 3 PTPN22 deficiency enhances TCR-mediated T cell proliferation. CellTrace Violet (CTV) labeled naive ($CD44^{lo}CD62L^{hi}$) T cells from the lymph nodes of *Ptpn22*$^{+/+}$ and *Ptpn22*$^{\Delta/\Delta}$ mice were stimulated with the indicated concentrations of plate-bound α-CD3ε plus α-CD28 (2 μg/mL) for 2 days at which stage the majority of resultant expanded T cells had taken on a $CD44^{hi}CD62L^{hi}$ central memory phenotype (data not shown) or for 4 days. On day 2 (A and C) or day 4 (B and D), blast formation was assessed (A and B), and cell numbers (A and B), and CTV dilution (C and D) were determined by flow cytometry. Representative results (means $\pm$ the SEM) from at least two independent experiments are shown. Significance in panels B and D was determined using two-way ANOVA (**, $P < 0.01$; ****, $P < 0.0001$).

detected in the spleens of aged *Ptpn22*$^{\Delta/\Delta}$ mice, also noted previously for *Ptpn22*$^{-/-}$ mice (23) (see Fig. S1d). Furthermore, TCR-induced PTK signaling, as assessed by monitoring for the tyrosine phosphorylation of TCR signaling intermediates, including ZAP-70 Y493 and LCK Y394 phosphorylation, was more pronounced in *Ptpn22*$^{\Delta/\Delta}$ effector T cells (see Fig. S4a and b) and accompanied by increased downstream mitogen-activated protein kinase (MAPK) signaling, as assessed by monitoring for ERK-1/2 phosphorylation (p-ERK1/2) by immunoblotting (see Fig. S4b) or by flow cytometry (Fig. 2A), as also seen in *Ptpn22*$^{-/-}$ effector T cells (23). Consistent with this, the expression of CD25 (Fig. 2B), the high-affinity receptor for interleukin-2 (IL-2) that is induced after TCR-induced T cell activation, as well as IL-2-induced STAT5 Y694 phosphorylation (Fig. 2C), were increased in *Ptpn22*$^{\Delta/\Delta}$ *in vitro* generated effector T cells (see Fig. S4a); by contrast STAT5 Y694 phosphorylation was not

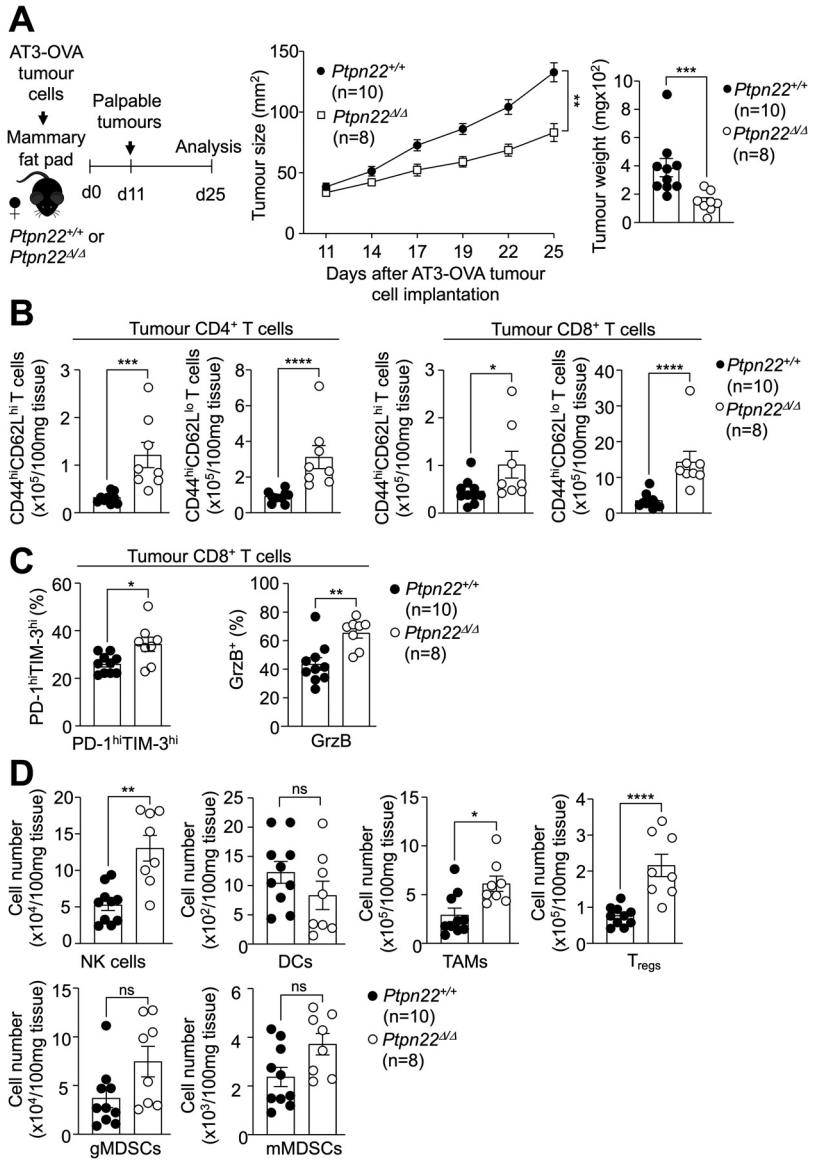

FIG 4 PTPN22 deficiency represses syngeneic tumor growth. (A) AT3-OVA tumor cells were orthotopically injected into the fourth inguinal mammary fat pads of age-matched *Ptpn22*$^{+/+}$ or *Ptpn22*$^{\Delta/\Delta}$ female C57BL/6 mice. Tumor growth was monitored and tumor weights determined. (B) Tumor infiltrating effector/memory (EM) CD44^{hi}CD62L^{lo} and central memory (CM) CD44^{hi}CD62L^{hi} CD4^{+} and CD8^{+} T cell numbers were determined by flow cytometry. (C) The proportions of PD-1^{hi}TIM-3^{hi}- and granzyme B-positive (GrzB^{+}) tumor-infiltrating CD8^{+} T cells were analyzed by flow cytometry. (D) Tumor-infiltrating immune cells, including NK1.1^{+}TCRβ- (NK cells), CD11c^{+} dendritic cells (DCs), CD11b^{+}F4/80^{hi}Ly6C^{-}Ly6G^{-} tumor-associated macrophages (TAMs), granulocytic CD11b^{+}F4/80$^{hi/lo}$Ly6C^{int}Ly6G^{+} (gMDSCs) and monocytic CD11b^{+}F4/80$^{hi/lo}$Ly6C^{+}Ly6G^{-} (mMDSCs) myeloid-derived suppressor cells and CD25^{+}Foxp3^{+} CD4^{+} regulatory T cells (T$_{regs}$) were analyzed by flow cytometry. Representative results (means $\pm$ the SEM) from at least two independent experiments are shown. In panels A to D, significance was determined using a two-tailed Mann-Whitney U test (*, $P < 0.05$; **, $P < 0.01$; ***, $P < 0.001$; ****, $P < 0.0001$).

increased in response to other cytokines, including IL-7 and IL-15 (see Fig. S5a and b). Finally, PTPN22 deficiency enhanced the expansion of lymph node naive T cells, as assessed by the formation of blasts, the dilution of CellTrace Violet (CTV) upon cell division, and the resultant increased cell numbers when the TCR was cross-linked with α-CD3/α-CD28 (Fig. 3). As the enhanced T cell expansion was evident after 4 days, but not after 2 days, when T cells stimulated with 2.5 μg/mL α-CD3 had already undergone 1 to 2 divisions (Fig. 3C and D) and differentiated into CD44^{hi}CD62L^{hi} memory T cells (data not shown), this is consistent

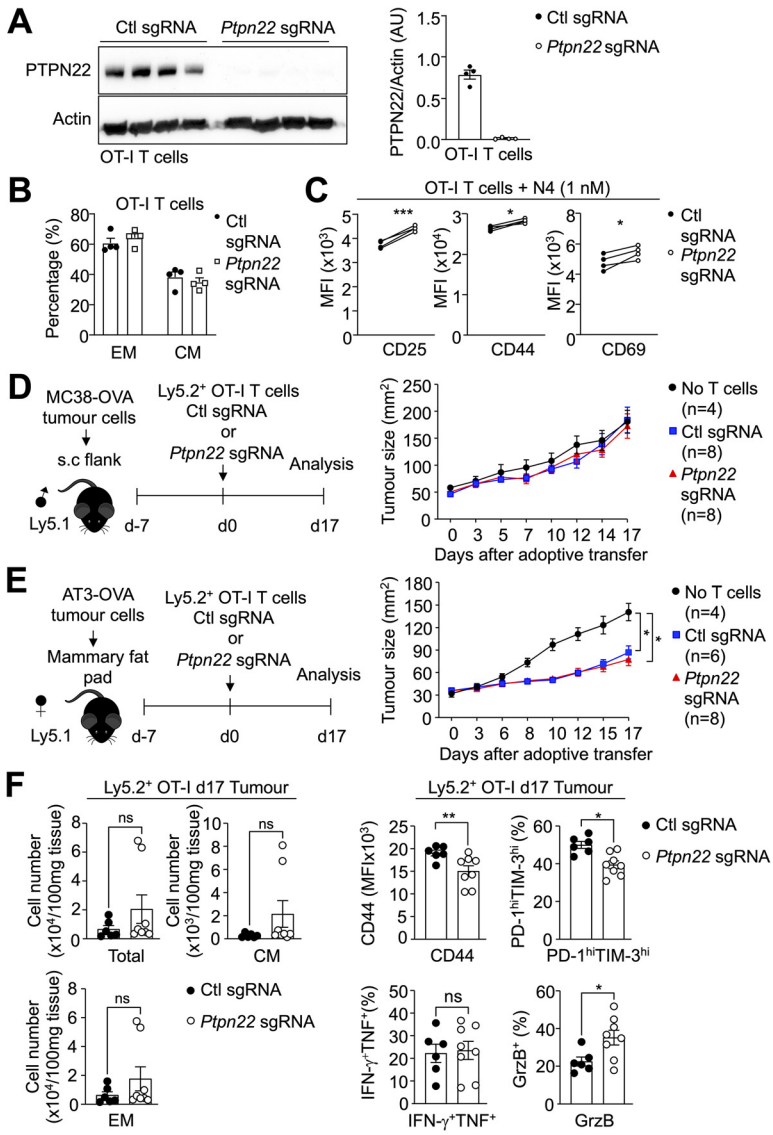

FIG 5 CRISPR/Cas9-mediated PTPN22 deletion does not enhance the antitumor activity of adoptively transferred OT-I CD8$^+$ T cells. Naive CD8$^+$ T cells were isolated from the spleens of Ly5.2$^+$ OT-I mice and PTPN22 was deleted using CRISPR RNP gene-editing. T cells were then expanded in the presence of cognate peptide antigen SII**N**FEKL (N4; 1 nM), IL-2 (5 ng/mL), and IL-7 (0.2 ng/mL) for 7 days before further analysis or adoptive transfer. (A) PTPN22 levels in OT-I cells electroporated with Cas9 and control (Ctl) or *Ptpn22* sgRNAs were assessed by immunoblotting. (B) OT-I T cell CD44^{hi} CD62L^{lo} effector memory (EM) and CD44^{hi}CD62L^{lo} central memory (CM) subsets were determined by flow cytometry. (C) OT-I cells were restimulated with N4 (1 nM) overnight, and CD25, CD44, and CD69 levels were analyzed by flow cytometry. (D to F) Control or PTPN22 deleted Ly5.2$^+$ CD8$^+$ OT-1$^+$ T cells were adoptively transferred into Ly5.1$^+$ mice bearing established subcutaneous (s.c.) (D) or established AT3-OVA mammary tumors (E and F), and tumor growth was monitored. (F) The number of Ly5.2$^+$ CD8$^+$ OT-1 tumor-infiltrating T cells with an EM CD44^{hi}CD62L^{lo} and CM CD44^{hi}CD62L^{hi} phenotype and PD-1, TIM-3, and CD44 levels were determined by flow cytometry. Tumor-infiltrating T cells were also stimulated with PMA/ionomycin in the presence of Golgi Stop/Plug and stained for intracellular IFN-γ and TNF. Intracellular granzyme B (GrzB) was detected in unstimulated tumor-infiltrating OT-1 T cells. In panel C, significance was determined using a Student paired *t* test; in panel E, significance was determined by using two-way ANOVA, and in panel F significance was determined by using a two-tailed Mann-Whitney U test (*, $P < 0.05$; **, $P < 0.01$; ***, $P < 0.001$).

with PTPN22 deficiency promoting TCR signaling and responses in effector/memory T cells, but not naive T cells, as reported previously (23). In line with this, PTPN22 deficiency also enhanced the TCR-mediated expansion of *in vitro* generated "rested effector" T cells that have a memory (CD44^{hi}CD62L^{hi}) phenotype (Fig. 2D; see also Fig. S4a). Taken together, these

results demonstrate that the *Ptpn22*$^{\Delta/\Delta}$ (C57BL/6) hypomorphs are for all intent and purposes null for PTPN22 and phenocopy *Ptpn22*$^{-/-}$ (C57BL/6) mice.

Global PTPN22-deficiency represses syngeneic mammary tumor growth. Previous studies have established that the global deletion of PTPN22 enhances antitumor immunity and can repress the growth of tumors that have abundant tumor-infiltrating lymphocytes (TILs) (28–30). Accordingly, before assessing whether PTPN22 deficiency might enhance the efficacy of CAR T cells, we tested whether the ablation of PTPN22 in *Ptpn22*$^{\Delta/\Delta}$ (C57BL/6) mice might enhance antitumor immunity and repress the growth of syngeneic tumors. To this end, we implanted ovalbumin (OVA)-expressing AT3 (AT3-OVA) murine mammary tumor cells (AT3 cells lack estrogen receptor, progesterone receptor and ErbB2 expression and are a model of triple negative breast cancer [32, 33]) into the inguinal mammary fat pads of *Ptpn22*$^{+/+}$ and *Ptpn22*$^{\Delta/\Delta}$ female mice (Fig. 4). PTPN22 deficiency repressed tumor growth (Fig. 4A), and this was accompanied by increased tumor-infiltrating CD4$^+$ and CD8$^+$ CD44^{hi}CD62L^{hi} central memory and CD44^{hi}CD62L^{lo} effector memory T cells (Fig. 4B); tumor-infiltrating CD8$^+$ T cells were more activated and cytotoxic, as assessed by monitoring for cell surface PD-1 and Tim-3 levels and intracellular granzyme B levels (Fig. 4C). Tumor-infiltrating mature natural killer (NK) cells that promote antitumor immunity were also significantly increased, whereas antigen-presenting CD11c$^+$ dendritic cells (DCs) that facilitate T cell activation trended lower and F4/80$^+$ CD11b$^+$ tumor-associated macrophages (TAMs) and CD4$^+$ CD25^{hi} T$_{regs}$ that can repress antitumor immunity were significantly increased (Fig. 4D); granulocytic and monocytic myeloid-derived suppressor cells (MDSCs) were not altered (Fig. 4D). The increased abundance of activated T cells and mature NK cells, as well as T$_{regs}$ within the tumor, was not a mere reflection of systemic differences in immune subsets, since lymphocyte numbers and T cell activation in the lymph nodes of contralateral mammary fat pads were only modestly, if at all, altered (see Fig. S6). Therefore, the global deletion of PTPN22 can repress the growth of syngeneic tumors, but this is accompanied by the recruitment of TILs that both promote and antagonize antitumor immunity. As such, the overall impact of immunotherapy approaches focused on systemically targeting PTPN22 to combat cancer might ultimately be dictated by the recruitment of TILs with potentially opposing effects on tumor growth.

PTPN22 deficiency does not enhance the antitumor activity of OT-I T cells. One immunotherapy approach by which to overcome the potential confounding effects of systemically targeting PTPN22 on antitumor immunity is adoptive T cell therapy. The adoptive transfer of autologous T cells expanded *ex vivo* and engineered to express high-affinity TCRs specific for defined tumor antigens has great potential in cancer therapy, especially if combined with gene-editing approaches to enhance function and promote persistence in nonautologous settings, with such approaches recently entering clinical trials (34). Accordingly, we next tested whether the deletion of PTPN22 might enhance the antitumor immunity of adoptively transferred CD8$^+$ T cells bearing the high-affinity OT-I TCR for the OVA peptide SIINFEKL (N4). In this case, we deleted PTPN22 in OT-I T cells with CRISPR ribonucleoprotein (RNP) gene editing (35, 36) using a short-guide RNA (sgRNA) targeting *Ptpn22* and thereon expanded the OT-I CD8$^+$ T cells with N4 peptide and IL-2 and IL-7 to generate a mix of CD44^{hi}CD62L^{lo} effector and CD44^{hi}CD62L^{hi} memory T cells (Fig. 5A and B). PTPN22 was effectively ablated in the resultant T cells, as assessed by immunoblot analysis (Fig. 5A), and this was associated with enhanced T cell activation (as assessed by the increased expression of CD44, CD25, and CD69) upon rechallenge with N4 peptide (Fig. 5C). Next, Ly5.2$^+$ congenically marked control or PTPN22-deficient OT-I effector and central memory T cells were adoptively transferred into immunocompetent Ly5.1$^+$ C57BL/6 mice bearing either established (30 to 40 mm^2) AT3-OVA mammary tumors in female mice or established (40 to 50 mm^2) OVA-expressing MC38 (MC38-OVA) colorectal tumors implanted into the flanks of male mice (Fig. 5D to F). The adoptive transfer of control OT-I T cells repressed AT3-OVA tumor growth, whereas OT-I T cells had no effect on the growth of MC38-OVA tumors (Fig. 5D and E; see also Fig. S7a and b). Irrespective, in each case, the adoptive transfer of PTPN22-deficient OT-I T cells had no additional effect on tumor growth (Fig. 5D and E) and did not affect the infiltration or increase the activation (as reflected by CD44, PD-1, and Tim-3 levels) of OT-I CD8$^+$ T cells in tumors (Fig. 5F; see also Fig. S7a). PTPN22 deficiency also did not enhance the cytotoxicity of infiltrating OT-I

$CD8^+$ T cells, at least as assessed by measuring intracellular TNF and IFN-γ levels, but increased granzyme B levels in OT-I $CD8^+$ T cells in AT3-OVA tumors (Fig. 5F; see also Fig. S7a). Nonetheless, these findings indicate that the targeting PTPN22 in adoptive cell therapy with T cells engineered to express high-affinity TCRs for tumor antigens is unlikely to be of any significant benefit in repressing tumor growth.

PTPN22 deficiency does not enhance the antitumor activity of murine α-HER2 CAR T cells. Next, we assessed whether PTPN22 deficiency might enhance the efficacy of adoptively transferred CAR T cells. First, we took advantage of a syngeneic tumor model in which the repression of tumor growth by murine CAR T cells is assessed in an immunocompetent setting. Specifically, we assessed the impact of PTPN22 deficiency on the cytotoxic activity of second-generation murine CAR T cells targeting the human orthologue of murine ErbB2/Neu, HER2 (37, 38). Control and *Ptpn22*$^{\Delta/\Delta}$ α-HER2 CAR T cells were generated as described previously (12) by retroviral means in activated splenic T cells cultured in the presence of IL-2 and IL-7 (Fig. 6A and B). PTPN22-deficiency did not significantly affect the generation of effector/memory versus central memory α-HER2 CAR T cells (Fig. 6C). However, in line with PTPN22 deficiency promoting CAR signaling, we found that CD25 and PD-1 levels (markers of enhanced TCR signaling and T cell activation) after challenge with HER2-expressing 24JK (HER2-24JK) sarcoma cells were enhanced by the deletion of PTPN22 (Fig. 6D). To determine whether the enhanced tumor cell-specific CAR T cell activation was sufficient to also enhance CAR T cell cytotoxicity, we monitored for (i) IFN-γ production after coculturing α-HER2 CAR T cells with 24JK versus HER2-24JK sarcoma cells, or (ii) the specific killing of 24JK-HER2 cells (Fig. 6E and F). We found that PTPN22 deficiency had no effect on α-HER2 CAR T cell cytotoxicity *in vitro* (Fig. 6E and F). These results indicate that the enhanced CAR T cell activation associated with the deletion of PTPN22 is not sufficient to enhance CAR T cell cytotoxicity. Nonetheless, we also assessed the impact of PTPN22-deficiency on the therapeutic efficacy of CAR T cells *in vivo*. To this end, we adoptively transferred mCherry$^+$ *Ptpn22*$^{+/+}$ or *Ptpn22*$^{\Delta/\Delta}$ α-HER2 CAR T cells into sublethally irradiated hosts bearing established (25 to 30 mm^2) orthotopic mammary tumors arising from the injection of syngeneic E0771 mammary tumor cells expressing the extracellular and transmembrane domains of HER2 (HER2-E0771) (Fig. 7A to D). HER2-E0771 cells were injected into the mammary fat pads of HER2 transgenic (TG) mice (39), so that HER2-expressing orthotopic tumors would be regarded as self and α-HER2 host immunity repressed. In the first instance, we adoptively purified CD44^{hi}CD62L^{hi} central memory $CD8^+$ CAR T cells since they exhibit superior engraftment and persistence (40) (Fig. 7A to C). Although *Ptpn22*$^{+/+}$ α-HER2 CAR T cells repressed tumor growth compared to untreated controls, the deletion of PTPN22 had no additional impact on tumor growth (Fig. 7A). In addition, PTPN22 deficiency did not significantly affect the infiltration of mCherry$^+$ CAR T cells into HER2-E0771 tumors (Fig. 7B), nor their tumor-specific activation, as assessed by monitoring for the expression of CD44 and PD-1 in CAR T cells in tumors versus lymphoid organs (Fig. 7C).

Previous studies have shown that effective tumor killing by $CD8^+$ CAR T cells is reliant on the presence of $CD4^+$ CAR T cells (40, 41). This is line with studies that have shown that $CD4^+$ T cell help is important for mounting effective CTL responses and antitumor immunity (42, 43). Since PTPN22 also negatively regulates TCR signaling in $CD4^+$ T cells (23) and recent studies have shown that $CD4^+$ T cells contribute to antitumor immunity in *Ptpn22*$^{-/-}$ mice (28), we also assessed whether the adoptive transfer of $CD4^+$ PTPN22-deficient α-HER2 CAR T cells along with $CD8^+$ PTPN22-deficient α-HER2 CAR T cells, might elicit superior tumor control than *Ptpn22*$^{+/+}$ CAR T cells (Fig. 6C and Fig. 7D). In this case we adoptively transferred both CD44^{hi}CD62L^{hi} central memory and CD44^{hi}CD62L^{lo} effector memory $CD4^+$ and $CD8^+$ CAR T cells (Fig. 6C and Fig. 7D). However, yet again we found that the suppression of tumor growth by PTPN22-deficient CAR T cells was not greater than that achieved with wild-type CAR T cells (Fig. 7D). Therefore, the deletion of PTPN22 in murine CAR T cells has no significant impact on CAR T cell efficacy in a solid tumor setting.

PTPN22 deficiency does not enhance the cytotoxicity of human α-LeY CAR T cells. Although PTPN22 deficiency had no impact on murine α-HER2 CAR T cell cytotoxicity, we sought to determine whether PTPN22 deletion might enhance the activation and cytotoxicity of human CAR T cells. Once more, we utilized CRISPR RNP gene editing and

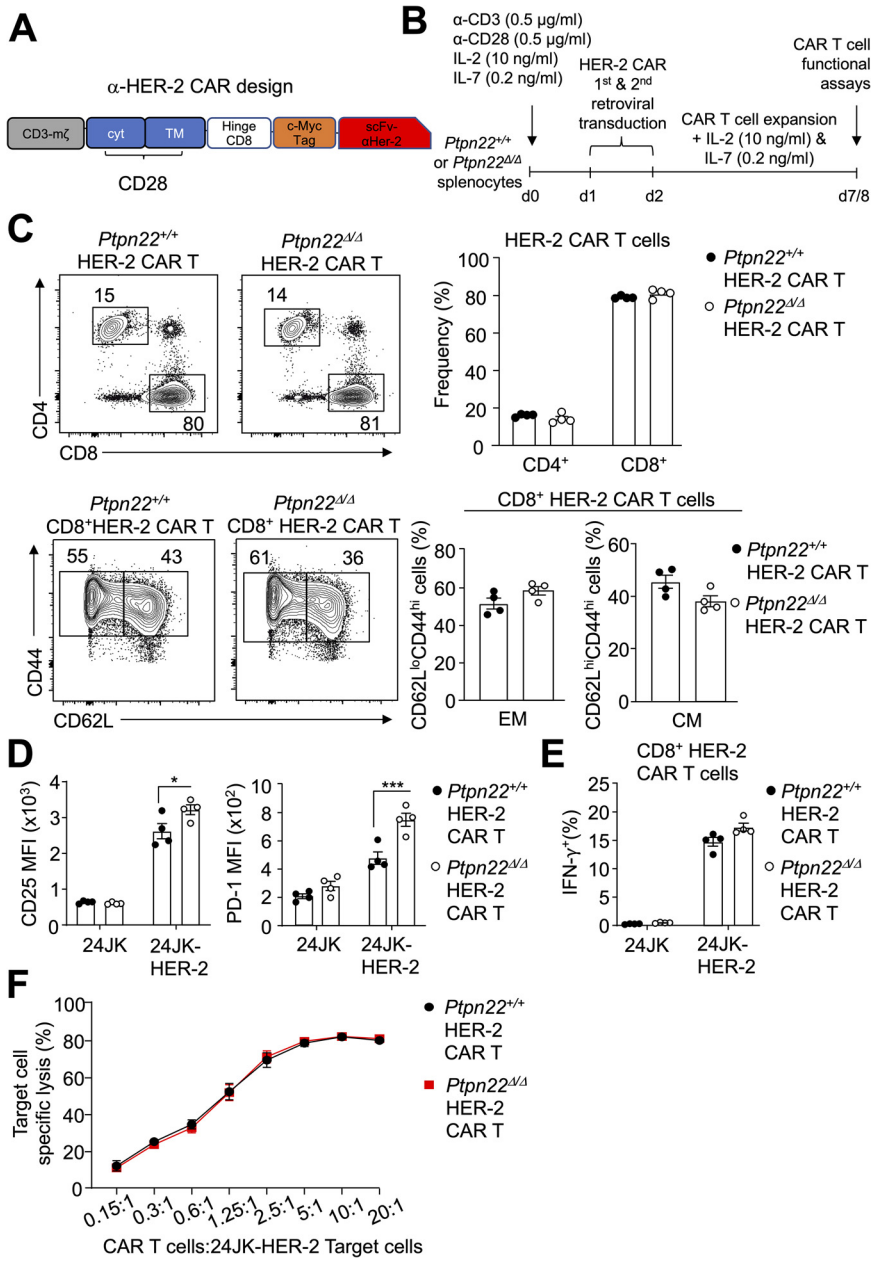

FIG 6 PTPN22 deficiency does not enhance the cytotoxicity of α-HER2 CAR T cells *in vitro*. Splenic lymphocytes were isolated from *Ptpn22*$^{+/+}$ and *Ptpn22*$^{\Delta/\Delta}$ C57BL/6 mice, activated, and expanded with α-CD3ε (0.5 μg/mL), α-CD28 (0.5 μg/mL), IL-2 (10 ng/mL), and IL-7 (0.2 ng/mL) and then transduced with retroviruses encoding the α-HER2 CAR. Cells were stained with antibodies for CD8, CD4, CD44, and CD62L and T cell populations analyzed by flow cytometry. (A) Schematic diagram of the α-HER2 CAR that is composed of an extracellular single-chain variable fragment (scFv) that recognizes the human orthologue of murine ErbB2/Neu (HER2) and the transmembrane (TM) and intracellular signaling domains (cyt) of CD28 and CD3ζ. (B) Protocol for generating *Ptpn22*$^{+/+}$ and *Ptpn22*$^{\Delta/\Delta}$ α-HER2 CAR T cells. (C) Representative dot plots and percentages of CD4$^+$ and CD8$^+$ T cells CD8$^+$ effector/memory (EM) and central memory (CM) α-HER2 CAR T cells. (D) *Ptpn22*$^{+/+}$ and *Ptpn22*$^{\Delta/\Delta}$ α-HER2 CAR T cells were cocultured with HER2$^+$ or HER2$^-$ 24JK tumor cells for 16 h. CAR T cells were then harvested and CD25 and PD-1 levels analyzed by flow cytometry. (E) *Ptpn22*$^{+/+}$ and *Ptpn22*$^{\Delta/\Delta}$ α-HER2 CAR T cells were cocultured with HER2$^+$ or HER2$^-$ 24JK tumor cells for 4 h in the presence of Golgi plug/stop and intracellular IFN-γ analyzed by flow cytometry. (F) *Ptpn22*$^{+/+}$ and *Ptpn22*$^{\Delta/\Delta}$ α-HER2 CAR T cells were cocultured with a 1:1 ratio mixture of 5 mM CTV-labeled (CTV^{bright}) HER2$^+$ 24JK tumor cells and 0.5 mM CTV-labeled (CTV^{dim}) HER2$^-$ 24JK tumor cells for 4 h. Antigen-specific killing was assessed by the relative decrease of CTV^{bright} HER2$^+$ 24JK tumor cells in comparison with CTV^{dim} HER2-24JK tumor cells by flow cytometry. In panel D, significance was determined by using a two-tailed Mann-Whitney U test (*, $P < 0.05$; ***, $P < 0.001$).

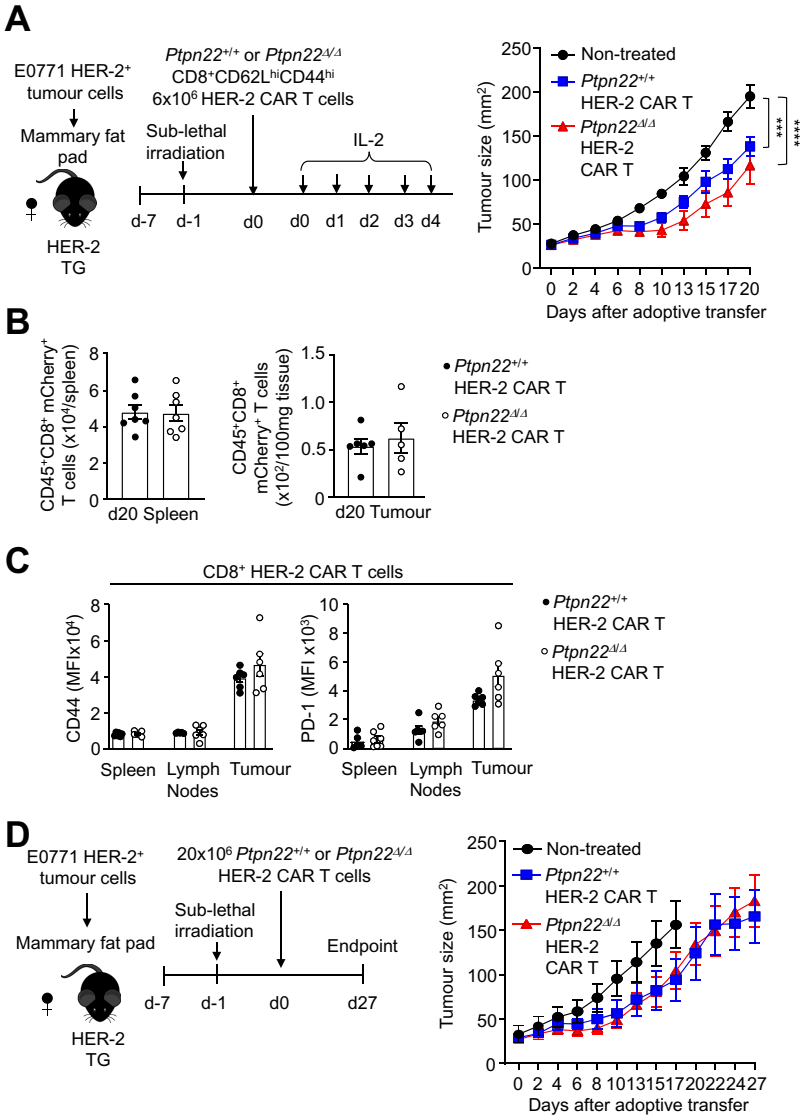

FIG 7 PTPN22 deficiency does not enhance the efficacy of α-HER2 CAR T cells *in vivo*. (A to C) E0771-HER2 mammary tumor cells (2×10^5) were injected into the fourth inguinal mammary fat pads of female HER2 transgenic (TG) mice. Six days after, when tumors were established, HER2 TG mice received total body irradiation (4 Gy), followed by the adoptive transfer of 6×10^6 FACS-purified $CD8^+$ $CD44^{hi}$ $CD62L^{hi}$ central memory α-HER2 CAR T cells generated from *Ptpn22*$^{+/+}$ versus *Ptpn22*$^{\Delta/\Delta}$ splenocytes. (A) Mice were injected with IL-2 (50,000 IU/day) on days 0 to 4 after adoptive CAR T-cell transfer, and tumor growth was monitored. (B) $mCherry^+$ HER2 CAR T cell numbers in tumor and spleens. (C) CD44 and PD-1 levels on $mCherry^+$ HER2 CAR T cells in tumors, spleens, or lymph nodes. (D) E0771-HER2 mammary tumor cells (2×10^5) were injected into the fourth inguinal mammary fat pads of female HER2 TG mice. Six days after, HER2 TG mice received total body irradiation (4 Gy), followed by the adoptive transfer of 20×10^6 *Ptpn22*$^{+/+}$ versus *Ptpn22*$^{\Delta/\Delta}$ $CD4^+$ and $CD8^+$ effector/memory and central memory α-HER2 CAR T cells, and tumor growth was monitored. Significance in panel A was determined by using two-way ANOVA (***, $P < 0.001$; ****, $P < 0.0001$).

electroporated human effector T cells, derived from peripheral blood mononuclear cells (PBMCs), with Cas9 and control or *PTPN22*-specific sgRNAs (Fig. 8A and B). CRISPR RNP targeting of *PTPN22* in T cells from 5 different donors almost completely ablated PTPN22 protein as assessed by immunoblotting (Fig. 8C). As in murine T cells, the deletion of PTPN22 enhanced the expansion (as assessed by CTV dilution) of human $CD8^+$ T cells after TCR cross-linking with α-CD3 (Fig. 8D). Next, we transduced PBMC-derived T cells from four different human donors with retroviruses encoding a second-generation human CAR targeting the Lewis Y (LeY) antigen that is expressed abundantly in a wide range of solid organ malignancies, but has limited expression in normal tissues (44, 45) (Fig. 9A to G); α-LeY CAR T cells

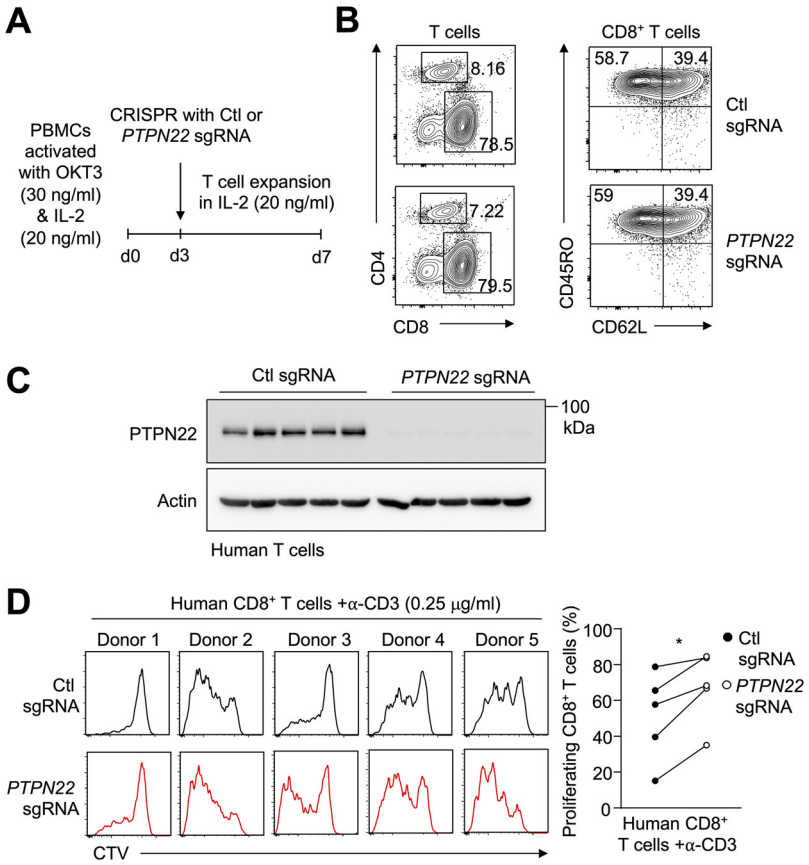

FIG 8 CRISPR/Cas9-mediated PTPN22 deletion in human T cells. PBMCs were stimulated with a-CD3ε (OKT3; 30 ng/mL) and IL-2 (20 ng/mL) for 3 days to activate and expand T cells. PBMC-derived T cells (5×10^6) were electroporated with Cas9 and control (Ctl) or *PTPN22* sgRNAs and cultured for another 4 days before any further assays. (A) Protocol schematic for the generation of PTPN22-deficient human T cells. (B) Representative subset analyses of PBMC-derived T cells. (C) PTPN22 levels in human T cells assessed by immunoblotting. (D) Control and PTPN22-deleted T cells were labeled with CellTrace Violet (CTV) and restimulated with OKT3 (0.25 μg/mL) for 5 days and CTV dilution analyzed by flow cytometry. Significance in panel D was determined using a Student paired *t* test (*, $P < 0.05$).

are currently in a phase 1b clinical trial (NCT03851146). We thereon electroporated CAR T cells with Cas9 precomplexed with either control or *PTPN22*-specific sgRNAs. CRISPR RNP editing of *PTPN22* in CAR T cells was efficient, so that little if any protein could be detected by immunoblotting (Fig. 9D). The antigen-specific cytotoxic potential of the resultant CAR T cells was assessed by monitoring for intracellular IFN-γ (required for tumor eradication by CAR T cells *in vivo* [41]) and TNF levels in CD8$^+$ CAR T cells upon coculture with human LeY$^+$ OVCAR3 ovarian carcinoma cells versus LeY$^-$ MDA-MB-435 breast cancer cells (Fig. 9E). IFN-γ and TNF were readily detected by flow cytometry when α-LeY CAR T cells were cocultured with LeY$^+$ OVCAR3 but not LeY$^-$ MDA-MB-435 tumor cells, but this was not affected by the deletion of PTPN22 (Fig. 9E). Consistent with this we found that antigen-induced CAR T cell activation, as assessed by monitoring for CD25 and CD69 levels, was not affected by the deletion of PTPN22 (Fig. 9F). In contrast the CRISPR RNP-mediated deletion of the tyrosine phosphatase PTPN2 (Fig. 10A), also known as TCPTP, which we have shown previously markedly enhances CAR T cell cytotoxicity and antitumor immunity (12), significantly increased the antigen-induced expression of IFN-γ and TNF (Fig. 10B). Consistent with the lack of effect on CAR T cell activation and cytotoxic potential, PTPN22 deficiency did not enhance the ability of α-LeY CAR T cells to kill LeY$^+$ OVCAR3 cells (Fig. 9G). Therefore, the deletion of PTPN22 in human CAR T cells has no significant impact on CAR T cell cytotoxicity.

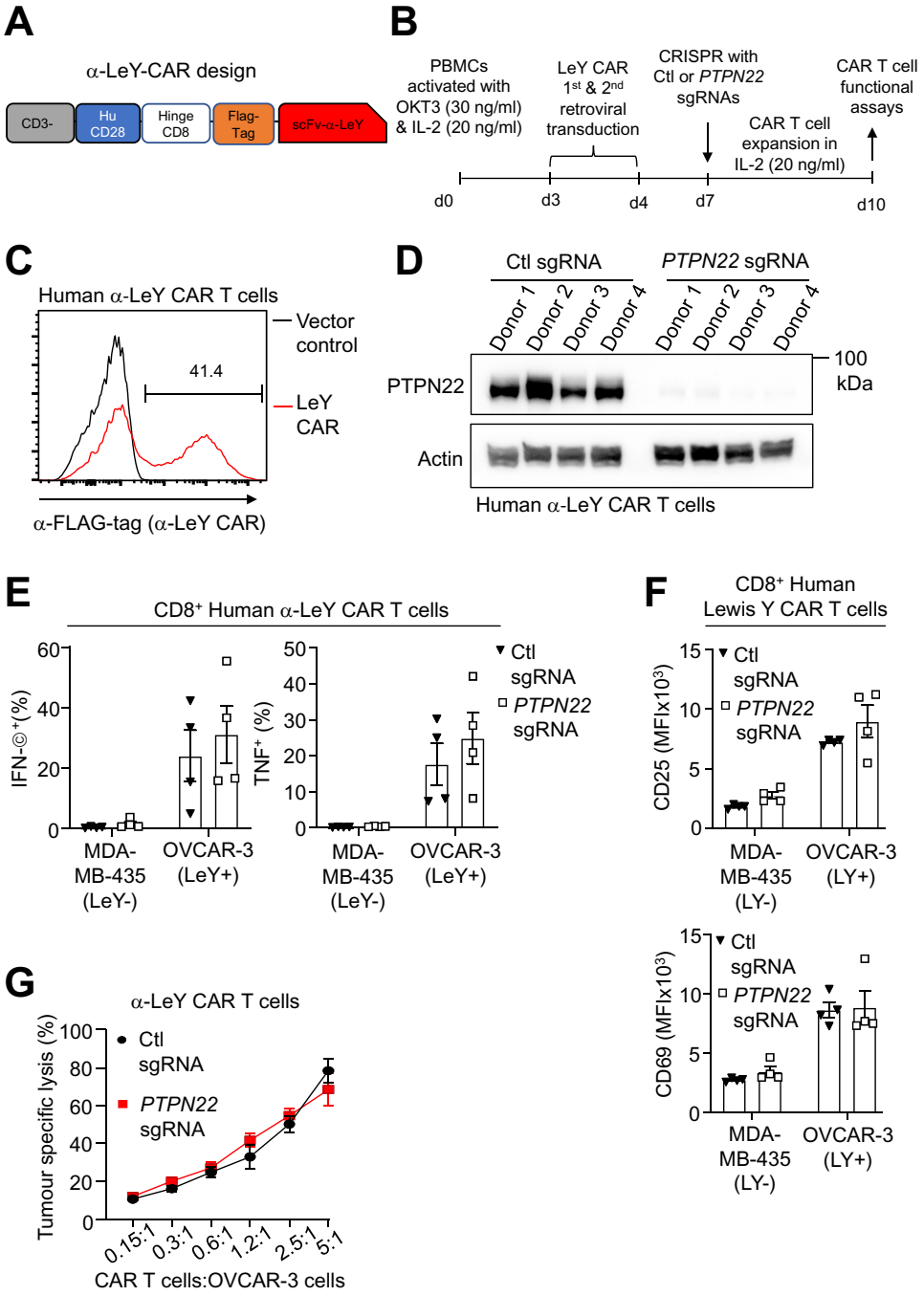

FIG 9 CRISPR/Cas9-mediated PTPN22 deletion does not enhance the antigen-specific cytotoxicity of a-LeY CAR T cells *in vitro*. PBMC-derived human T cells from four independent donors were stimulated with OKT3 (30 ng/mL) and IL-2 (20 ng/mL) for 3 days. On days 3 to 4, human T cells were transduced with retroviruses encoding the a-LeY CAR. On day 7, transduced cells were electroporated with Cas9 and control (Ctl) or *PTPN22* sgRNAs and cultured for another 7 days in media supplemented with IL-2 (20 ng/mL). (A) Schematic diagram of the α-LeY CAR structure. (B) Protocol schematic for the generation of PTPN22-deficient human α-LeY CAR T cells. (C) Retroviral transduction efficiency assessed by flow cytometry staining for the FLAG tag to identify α-LeY CAR$^+$ cells. (D) PTPN22 levels in human α-LeY CAR T cells assessed by immunoblotting. (E) Control or PTPN22 deleted α-LeY CAR T cells were cocultured with the LeY-expressing ovarian cancer cell line OVCAR3 or the LeY-negative breast cancer cell line MDA-MB-435 in the presence of Golgi Plug/Stop for 5 h, and intracellular IFN-γ and TNF levels were analyzed by flow cytometry. (F) Control or PTPN22 deleted α-LeY CAR T cells were cocultured with LeY-expressing OVCAR3 cells or the LeY-negative MDA-MB-435 cells, and mean fluorescence intensities (MFI) for CD25 and CD69 were determined by flow cytometry. (G) OVCAR3 cells (1×10^6) were labeled for 60 min with 100 μCi of ^{51}Cr and then cocultured with α-LeY CAR T cells at the indicated effector/target ratios. Supernatants were harvested after 4 h, ^{51}Cr levels analyzed using a gamma counter, and tumor-specific lysis was determined. The results shown are representative of two independent experiments.

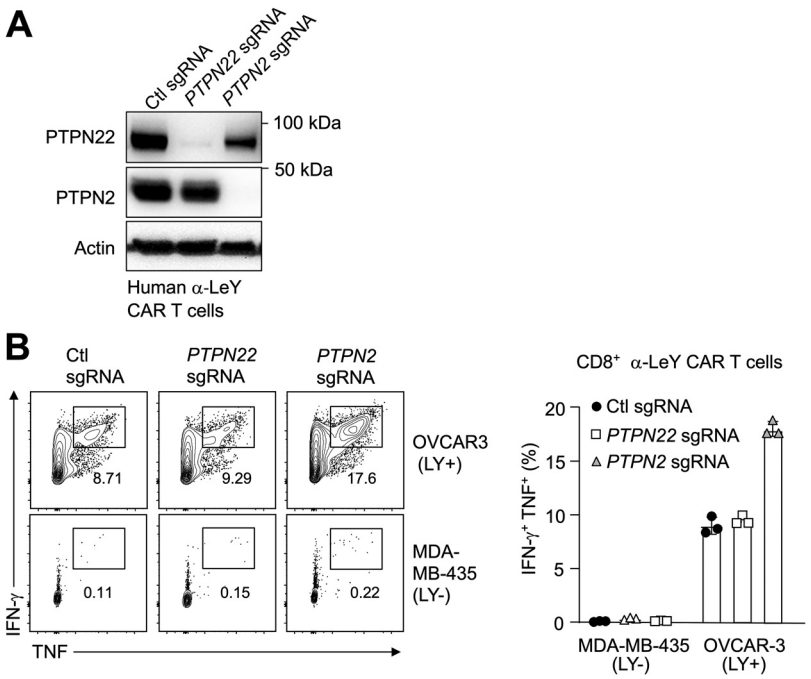

FIG 10 CRISPR/Cas9-mediated PTPN2 but not PTPN22 deletion in α-LeY CAR T cells enhances cytotoxic potential. PBMC-derived human T cells were stimulated with OKT3 (30 ng/mL) and IL-2 (20 ng/mL) for 3 days. On days 3 to 4, human T cells were transduced with retroviruses encoding the α-LeY CAR. On day 7, transduced cells were electroporated with Cas9 and control (Ctl), *PTPN2*, or *PTPN22* sgRNAs and cultured for another 7 days in media supplemented with IL-2 (20 ng/mL). (A) PTPN2 and PTPN22 levels in human α-LeY CAR T cells were assessed by immunoblotting. (B) Control, PTPN2-deleted, or PTPN22-deleted α-LeY CAR T cells were cocultured with the LeY-expressing ovarian cancer cell line OVCAR3 or the LeY-negative breast cancer cell line MDA-MB-435 in the presence of Golgi Plug/Stop for 5 h, and intracellular IFN-γ and TNF levels were analyzed by flow cytometry. The results shown are representative of two independent experiments.

DISCUSSION

Approaches that enhance the ability of T cells and CAR T cells to infiltrate solid tumors, become activated and overcome immune suppression, while avoiding T cell exhaustion stand to transform cellular immunotherapies. Notably, the advent of CRISPR/Cas9 gene editing affords unprecedented opportunities for deleting T cell inhibitory receptors, such as PD-1 (34) and the adenosine G-protein-coupled receptor $A_{2A}R$ (46), enzymes such as PTPN2 that tune T cell responses (12, 16) and transcription factors such as TOX that orchestrate T cell exhaustion (47, 48) to enhance the efficacy of adoptively transferred tumor antigen-specific T cells and CAR T cells. Indeed, CRISPR targeting has already been used safely in the clinic to genetically modify adoptively transferred T cells (34, 49). In this study, we explored the therapeutic potential of targeting the autoimmunity-linked tyrosine phosphatase PTPN22 in adoptive T cell and CAR T cell immunotherapy. Although PTPN22's role in establishing immune tolerance is well established (21, 22), and recent studies have shown that its global deletion can promote antitumor immunity (28) and enhance the ability of T cells to overcome T_{reg}-mediated immune suppression and respond to tumors with low-affinity antigens (29, 30), our results suggest that targeting PTPN22 is unlikely to be of any significant benefit in adoptive T cell therapies, especially those utilizing CAR T cells.

Cubas et al. (28) reported that although global PTPN22 deletion does not affect the growth of subcutaneous MC38 colon adenocarcinomas, it can enhance the response to PD-1 checkpoint blockade and repress tumor growth. On the other hand, the global deletion of PTPN22 resulted in the spontaneous repression of subcutaneous Hepa1-6.x1 tumors that are normally highly enriched in $CD8^+$ T cells; PTPN22 deficiency did not affect overall T cell numbers in Hepa1-6.x1 tumors, but it did promote $CD8^+$ T cell activation and T cells were required for the repression of tumor growth (28). In our studies, we found that the growth immunogenic AT3-OVA tumors implanted into *Ptpn22*$^{\Delta/\Delta}$ mice was also significantly reduced and that

this was accompanied by the increased recruitment of $CD4^+$ and $CD8^+$ central memory and/or effector/memory T cells. Notably, infiltrating PTPN22-deficient $CD8^+$ T cells were more activated and cytotoxic. In addition, we found that PTPN22 deficiency not only increased the recruitment T cells and NK cells that elicit antitumor immunity but also increased TAMs and T_{regs}. Therefore, the systemic inhibition of PTPN22 might facilitate antitumor immunity or enhance the response to immune checkpoint blockade, but such effects might be dictated by the immunogenicity of the tumor and the abundance of T cells relative to other TILs (28–30). Nonetheless, recent studies have shown that the systemic administration of a PTPN22-selective inhibitor can partially repress the growth of syngeneic tumor xenografts in mice and enhance the response to PD-1 blockade by both remodeling the macrophage compartment, so that it is predominated by proinflammatory M1-like phenotype macrophages and by enhancing T cell-mediated antitumor immunity (50).

Some studies have suggested that targeting of PTPN22 may also be beneficial for enhancing the antitumor immunity of adoptively transferred T cells. Brownlie et al. (30) have shown that *Ptpn22*$^{-/-}$ $CD8^+$ T cells are resistant to the immunosuppressive effects of transforming growth factor β (TGFβ) and that adoptively transferred *Ptpn22*$^{-/-}$ OT-I $CD8^+$ T cells specific for the OVA peptide SII**N**FEKL can effectively repress the growth OVA-expressing EL4 lymphoma tumors that specifically secrete TGFβ. However, the same group has subsequently shown that adoptively transferred effector *Ptpn22*$^{-/-}$ OT-I $CD8^+$ T cells are no more efficient at repressing the growth of OVA-expressing ID8 ovarian carcinoma cells than control OT-I T cells, but effectively repress the growth of ID8 cells expressing a SII**V**FEKL OVA variant (K_D for OT-I TCR $>$ 1 mM) with an affinity for OT-I considerably lower than that for SII**N**FEKL (K_D for OT-I TCR of 54 μM) (29). Endogenous T cells can recognize both neo-antigens, which would involve high-affinity interactions, as well as aberrantly expressed self-antigens with very low affinities (51–53). It is possible that PTPN22 targeting might enhance the antitumor activity of T cells in a setting of heightened TGFβ secretion and/or enhance the activity of T cells recognizing very low-affinity self-antigens on tumors. However, this might occur at the expense of promoting overt autoimmunity. Irrespective, autologous T cell therapies with engineered T cells generally involve the use of T cells bearing TCRs that recognize tumor antigens with high affinity (34, 54). In our studies, adoptively transferred $CD44^{hi}$ $CD62L^{lo}$ effector/memory and $CD44^{hi}CD62L^{hi}$ central memory OT-I $CD8^+$ T cells deficient for PTPN22 were no more effective in repressing the growth of OVA-expressing AT3 mammary or MC38 colorectal tumors than control OT-I $CD8^+$ T cells. Thus, our studies suggest that PTPN22 may not be an ideal target for enhancing the therapeutic efficacy of adoptively transferred $CD8^+$ T cells bearing high-affinity TCRs for solid tumor antigens.

Anti-CD19 CAR T cells were first approved by the FDA for the treatment of B-ALL and aggressive lymphoma in 2017 (55). In this context, CAR T cells have shown remarkable clinical efficacy and established curative potential (6, 10). However, this has not been realized for many other malignancies, in particular solid organ malignancies (5, 6). Beyond the complications associated with tumor heterogeneity and the challenge of avoiding on-target off-tumor toxicities, CAR T cells infiltrating solid tumors also need to operate in a hostile immunosuppressive tumor microenvironment and overcome the development of exhaustion otherwise arising from persistent antigen engagement and CAR T cell activation (5, 6). Numerous strategies have been proposed by which to overcome these and other challenges (5–7). Our own recent studies have shown that the deletion of PTPN2 in α-HER2 CAR T cells can markedly enhance the efficacy of adoptively transferred CAR T cells and facilitate the eradication of large $HER2^+$ mammary tumors (12). This was associated with the increased homing of CAR T cells to CXCL9/10-expressing mammary tumors and enhanced tumor-specific CAR T cell activation and cytotoxicity attributable to the promotion of both CAR-LCK and IL-2/STAT5 signaling (12). However, other studies have shown that the deletion of PTPN2 and the promotion of IFNAR1/STAT1 signaling can also overcome T cell exhaustion to facilitate antitumor immunity (56), but this has not been assessed in the context of CAR T cells. Nonetheless, although PTPN22 deficiency also promoted TCR signaling and IL-2-induced STAT-5 signaling in effector T cells and PTPN22 has been shown to attenuate IFNAR1 signaling in immune cells (57), the deletion of PTPN22 in murine α-HER2 CAR T cells had no impact on CAR T cell

cytotoxicity and antitumor immunity. Similarly, the deletion of PTPN22 in human α-LeY CAR T cells had no effect on antigen-specific cytotoxicity; in contrast, CRISPR targeting of PTPN2 significantly enhanced α-LeY-induced CAR T cell cytotoxic potential, as reflected by the increased expression of IFN-γ and TNF. The reasons for this are not clear, but probably relate to the principal impact of PTPN22 deficiency on T cell responses to lower affinity antigens (29, 30, 58) and the extent to which PTPN22 deficiency may otherwise enhance TCR/CAR or cytokine signaling, when to compared to PTPs such as PTPN2 (12) or PTP1B (59). We and others have shown that the deletion of PTPN2 enhances responses to both low- and high-affinity antigens (12, 16, 17, 56) and that the deletion of PTPN2 in OT-I CD8$^+$ T cells can negate the need for CD4$^+$ T cell help (60, 61) and enhance the ability of CD8$^+$ T cells to repress the growth of OVA-expressing mammary tumors and melanomas (12). Similarly, we have shown that the deletion of PTP1B can promote IL-2/IL-15-induced STAT-5 signaling and the clonal expansion and antitumor activity of CD8$^+$ T cells (59). Moreover, we have shown that the deletion of either PTPN2 or PTP1B can markedly enhance the therapeutic efficacy of adoptively transferred α-HER2 CAR T cells (12, 59). Nonetheless, although the deletion of PTPN22 alone might not enhance responses to high-affinity antigens, recent studies have shown that engrafted PTPN22-deficient memory T cells can prevent the establishment of implanted tumors (29). Therefore, it remains to be determined if the combined targeting of PTPN2 or PTP1B together PTPN22 in adoptively transferred T cells and/or CAR T cells might ultimately provide a means for both promoting tumor eradication and preventing reemergence.

In summary, in this study we have generated PTPN22-deficient mice and taken advantage of CRISPR/Cas9 genome editing to explore the therapeutic potential of targeting PTPN22 in adoptive T cell/CAR T cell therapy. Although global PTPN22 deletion may enhance antitumor immunity (28) and the response of effector T cells to low-affinity antigens (29, 30, 58), our studies demonstrate that CRISPR targeting of PTPN22 in itself is insufficient to enhance the antitumor activity of adoptively transferred T cells targeting high-affinity tumor antigens or the efficacy of CAR T cells in solid tumors.

MATERIALS AND METHODS

Materials. Hamster α-mouse CD3ε (145-2C11) and hamster α-mouse CD28 (clone 37.51) were purchased from BD Biosciences. Mouse α-human CD3ε (OKT3) was from eBioscience; α-phospho-STAT5 (Tyr694) (D47E7) XP, rabbit α-phospho-p44/42 MAPK (Erk1/2) (Thr202/Tyr204) (D13.144E) XP, rabbit α-phospho ZAP-70 (Tyr493), mouse α-ZAP-70, and rabbit monoclonal α-PTPN22 (D6D1H) were from Cell Signaling Technology; rabbit α-phospho-Lck (Y394) (sc-101728) and mouse α-Lck (sc-433), α-ERK2 (sc-1647) and α-actin (sc-1616) were from Santa Cruz Biotechnology Inc.; α-actin (clone ACTN05) was from Thermo Fisher Scientific and mouse α-human PTPN2 (CF4-1D) from Calbiochem. Recombinant human IL-2, murine IL-7, and IL-15 used for T-cell stimulations and for the generation of CAR T cells were purchased from Lonza, SIINFEKL peptide (OVA257-264) from Auspep, RetroNectin from TaKaRa, and DNase I from Sigma-Aldrich. Fetal bovine serum (FBS) was purchased from Thermo Scientific, Dulbecco phosphate-buffered saline (d-PBS), RPMI 1640, Dulbecco modified Eagle medium (DMEM), minimal essential medium (MEM) nonessential amino acids, and sodium pyruvate were obtained from Invitrogen, and collagenase type IV was obtained from Worthington Biochemical.

Mice. Mice were maintained on a 12-h light/12-h dark cycle in a temperature controlled high-barrier facility with free access to food and water. C57BL/6J and female B6.SJL-*Ptprc*^{a} *Pepc*^{b}/BoyJ (Ly5.1) mice were purchased from the Walter and Eliza Hall Institute (WEHI; Parkville, Victoria, Australia) or the Animal Resources Centre (Perth, Western Australia). Human HER2 (C57BL/6) transgenic (TG) have been described previously (12).

Mice with a global deficiency in PTPN22 (referred to as *Ptpn22*$^{\Delta/\Delta}$ mice) were generated on a C57BL/6J background using CRISPR/Cas9 genome editing. These mice were generated in the course of generating PTPN22 R619W mutant mice. The CRISPR Design site (http://crispr.mit.edu/) was used to identify guide RNA target sequences close to the targeting site, amino acid 619, of the mouse gene *Ptpn22*; the following guide RNA sequence was used: 5′-AAAGACTCGGGTGTCCGTTC-3′. Complementary oligonucleotides corresponding to the RNA guide target sites were annealed and cloned into BbsI (NEB) digested plasmid pX330-U6-Chimeric_BB-CBh-hSpCas9 (Addgene). Single-guide RNA (sgRNA) was generated using a HiScribe T7 Quick High Yield RNA synthesis kit (NEB) according to the manufacturer's instructions. The sgRNA was purified using an RNeasy minikit (Qiagen), and Cas9 mRNA was purchased from Sigma. A single-stranded oligonucleotide designed to change the **C**GG codon, coding for R619, to **T**GG introducing the R619W mutation was ordered from Integrated DNA Technologies (IDT) and used as a homology directed repair (HDR) template. It also contained a base change to introduce a silent mutation (C to A) to alter the PAM site from GGG to GTG to prevent Cas9 digestion of the HDR oligonucleotide; the following repair oligonucleotide was used: 5′-CTATTACTTGGTTAGCTCCTTCTCGGAGGACA GATGATGAAATCCCACCGCCACTCCCTGAATGGACACCCGAGTCTTTTATTGTGGTTGAGGAAGCCGGTGAGTACAGTCA GTAAGTATGAAGTG-3′. Cas9 mRNA (30 ng/μL), sgRNA (15 ng/μL), and the homology directed repair template (30 ng/μL) were microinjected into the pronucleus of C57BL/6J zygotes at the pronuclei stage. Injected zygotes

were transferred into the uteruses of pseudo pregnant females. Gene-editing events in resultant founders were assessed by sequencing PCR products of the targeted site; the following forward (5′-TTGCCTAGAGTAAGCA AATGCAA-3′) and reverse (5′-AAAGGAGGC AGATGGATGCG-3′) primers were used amplify a product of 292 bp. In addition, to generating the point mutant mice, we generated mice that were the product of nonhomologous end-joining. Specifically, we identified mice with an adenine (A) insertion between c1854 and 1855. The frameshift resulted in an R619T substitution and introduced a stop codon after residue 628. These mice were crossed onto C57BL/6J mice, germ line transmission confirmed and then crossed to each other. Age- and sex-matched C57BL6/J mice were used for all experiments. All experiments were performed in accordance with the NHMRC Australian Code of Practice for the Care and Use of Animals. All protocols were approved by Monash University School of Biomedical Sciences Animal Ethics Committee (ethics number MARP/2012/066/BC) or the Peter MacCallum Animal Ethics and Experimentation Committee (ethics number E604).

Cell lines. The C57BL/6 mouse breast carcinoma cell line E0771 was a gift from Robin Anderson (Peter MacCallum Cancer Centre) (62), and the C57BL/6 mouse sarcoma cell line 24JK was a gift from Patrick Hwu (NIH, Bethesda, MD) (63). The corresponding cells lines engineered to express green fluorescent protein and the extracellular and transmembrane domains of human HER2 have been described previously (64) and are referred to as E0771-HER2 and 24JK-HER2. The C57BL/6 mouse mammary tumor cell line AT-3 engineered to express chicken ovalbumin (AT-3-OVA) or the mouse colon carcinoma cell line MC38 engineered to express chicken ovalbumin (MC38-OVA) have been described previously (12, 59). The viral packaging cell lines GP+E86 and PG13 have been described previously (37, 65, 66). The human ovarian adenocarcinoma cell line OVCAR3 (HTB-161TM) and the human breast cancer cell line MDA-MB-435 (HTB-219TM) were obtained from American Type Culture Collection (ATCC; Manassas, VA). The retroviral cell lines GP+E86 and PG13 and the tumor cell lines E0771-HER2, OVCAR-3, and MDA-MB-435 were cultured and maintained in RPMI 1640 (Gibco/Life Technologies) supplemented with 10% (vol/vol) heat-inactivated FBS, 2 mM L-glutamine, 1 mM sodium pyruvate, 10 mM HEPES, 100 U/mL penicillin, and 100 μg/mL streptomycin. The AT3-OVA, MC38-OVA, 24JK, and 24JK-HER2 cell lines were maintained in high-glucose DMEM (Gibco/Life Technologies) supplemented with 10% (vol/vol) heat-inactivated FBS, 2 mM L-glutamine, 1 mM sodium pyruvate, 10 mM HEPES, 100 U/mL penicillin, and 100 μg/mL streptomycin.

Flow cytometry. Single cell suspensions from spleens, lymph nodes, livers, and lungs were obtained as described previously (16). For the detection of intracellular cytokines, T cells were fixed and permeabilized with a BD Cytofix/Cytoperm kit according to the manufacturer's instructions. For the detection of intracellular FoxP3, a Foxp3/transcription factor staining buffer set (eBioscience) was used according to the manufacturer's instructions. Cells were acquired using LSRII (BD Biosciences, San Jose, CA), Fortessa (BD Biosciences), or Symphony (BD Biosciences). For fluorescence-activated cell sorting (FACS), cells were purified using either BD FACSAria II, BD FACSAria Fusion 3, or BD FACSAria Fusion 5 instruments. Data were analyzed with FlowJo10 software (Tree Star, Inc.). For cell quantification, a known number of Flow-Count Fluorospheres (Beckman Coulter) were added to samples before analysis.

The following antibodies raised against mouse antigens (obtained from BD Biosciences, BioLegend, Invitrogen, or eBioscience) were used for flow cytometry: PerCP-Cy5.5 or PE-Cy7-conjugated CD4 (RM4-5), BUV395 or Pacific Blue-conjugated-conjugated CD8 (53-6.7); PerCP-Cy5.5- or PE-conjugated CD25 (P61), BV711-conjugated CD11b (M1/70), APC- or V450-conjugated CD11c (N418), PE-conjugated CD19 (1D3), BV786 or FITC-conjugated CD44 (IM7), APC-conjugated CD45 (30-F11), FITC-conjugated CD45.1 (Ly5.1; A20), PE- or APC-Cy7-conjugated CD45.2 (Ly5.2; 104), BUV737 or APC-conjugated CD62L (Mel-14), BV510-conjugated CD69 (H1.2F3), PE-Cy7-conjugated CD279 (PD-1, RMP1-14), BV711-conjugated CD366 (TIM-3, RMT3-23), FITC- or PE-Cy7-conjugated Ly6C (HK1.4), APC-Cy7- or FITC-conjugated Ly6G (1A8), PE-Cy7-conjugated NK1.1 (PK136), BV605-conjugated TCR (H57-597), PE-Cy7-conjugated IFN-γ (XMG1.2), APC-conjugated TNF (MP6-XT22), Alexa Fluor 647-conjugated granzyme B (GB11), and FITC-conjugated FoxP3 (FJK-16s).

The following antibodies raised against human antigens (obtained from BD Biosciences, Invitrogen, BioLegend, and Miltenyi Biotec) were used for flow cytometry: PE-Cy7-conjugated CD4 (SK3), FITC-conjugated CD8 (BW135/80), APC-H7-conjugated CD8 (SK1), PE-conjugated α-FLAG (DYKDDDDK) Tag (L5), FITC-conjugated-CD45RO (UCHL1), BV711-conjugated CD62L (SK11), PE-Cy7-conjugated IFN-γ (4S.B3), and APC-conjugated-TNF (MAb11).

Immunoprecipitation of PTPN22. Splenocytes (5×10^7) from *Ptpn22*$^{+/+}$ and *Ptpn22*$^{\Delta/\Delta}$ mice were lysed in 250 μL of immunoprecipitation lysis buffer (50 mM Tris [pH 7.5], 1% [wt/vol] NP-40, 150 mM NaCl, 50 mM NaF) plus protease inhibitors (5 μg/mL leupeptin, 1 μg/mL pepstatin A, 1 μg/mL aprotinin, 1 mM benzamidine, 2 mM phenylmethylsulfonyl fluoride) for 30 min on ice. The lysates were precleared with 50 μL of Pansorbin cells (Sigma-Aldrich) for 30 min at 4°C. Lysates were centrifuged at 4°C for 5 min at 16,000 $\times$ *g*, and PTPN22 was immunoprecipitated from the clarified supernatants with 5 μL of α-PTPN22 (D6D1H) for 4 h at 4°C. Immune complexes were collected on 10 μL of protein G+A agarose (Merck) for 60 min at 4°C, washed with ice cold-lysis buffer, and then either resolved by SDS-PAGE and immunoblotted for PTPN22 or processed for PTP activity assays.

PTP activity assays. PTPN22 or PTPN22Δ immunoprecipitates were pelleted (2,500 $\times$ *g*, 5 min), washed twice in ice-cold IP lysis buffer without NaF, washed once in ice-old STE buffer (10 mM Tris-HCl [pH 7.8], 10 mM NaCl, 1 mM EDTA), and washed once in ice-old phosphatase assay buffer (24 mM HEPES, 120 mM NaCl), and then beads were resuspended in 40 μl of freshly prepared *p*-nitrophenyl phosphate (pNPP) reaction buffer (24 mM HEPES [pH 7.4], 150 mM NaCl, 12.5 mM pNPP, 6.25 mM DTT; Sigma), followed by incubation at 37°C for 4 h. Where indicated, 1 mM $NaVO_3$ was added to specifically inhibit PTP activity. Reactions were quenched with 1 mL of 0.2 M NaOH. Beads were pelleted (2,500 $\times$ *g*, 30 s), and 200-μL portions of the supernatants transferred to flat-bottom 96-well plates and the *p*-nitrophenylene anion product measured at an absorbance of 405 nm using a plate reader.

Immunohistochemistry. Formalin-fixed and paraffin-embedded spleen sections were stained with PNA (biotinylated peanut agglutinin α-mouse B-1075; Vector Laboratories) for 1 h and then incubated with streptavidin-HRP (Biocare Medical) for 20 min. DAB (3,3′ diaminobenzidine; Biocare Medical) was used as a chromogen and nuclei were counterstained with hematoxylin and eosin. An Olympus Bx61 microscope was used for visualization images and a RT SE SPOT camera with SPOT Advanced software v4.6 (Diagnostics Instruments) used to obtain images.

Generation of rested effector T cells. To generate rested effector T cells, 96-well U-bottom plates were coated with α-CD3ε (5 μg/mL) and α-CD28 (5 μg/mL) in PBS for 2 h at 37°C. Single lymph node cell suspensions (300,000/200 μL) were incubated for 3 days in complete T cell medium at 37°C. T cells were harvested and washed twice in PBS and rested in 96-well U-bottom plates (300,000/200 μL) in RPMI 1640 medium (Gibco/Life Technologies, Grand Island, NY) supplemented with 10% (vol/vol) heat-inactivated FBS, 2 mM L-glutamine, 0.1 mM MEM nonessential amino acids, 1 mM sodium pyruvate, 10 mM HEPES, 100 U/mL penicillin, 100 μg/mL streptomycin, 0.2 ng/mL IL-7, and 10 ng/mL IL-15 at 37°C and 5% CO_2 for 2 days.

Signaling assays. For TCR signaling assays *in vitro* generated rested effector T cells (5×10^6 to 10×10^6) were incubated with hamster α-mouse CD3ε (145-2C11) (1 μg/mL) in 500 μL of RPMI 1640 supplemented with 1% (vol/vol) FBS for 30 min on ice. Cells were washed once with ice cold RPMI 1640 and supernatant was aspirated. Cells were then incubated with goat α-hamster IgG(H+L) (20 μg/mL) antibody (Sigma-Aldrich) for the indicated times at 37°C. Cells were washed with ice-cold PBS and lysed in radioimmunoprecipitation assay buffer (50 mM HEPES [pH 7.4], 1% [vol/vol] Triton X-100, 1% [vol/vol] sodium deoxycholate, 0.1% [vol/vol] SDS, 150 mM NaCl, 10% [vol/vol] glycerol, 1.5 mM $MgCl_2$, 1 mM EGTA, 50 mM NaF, 1 mM sodium vanadate) plus protease inhibitors (5 μg/mL leupeptin, 1 μg/mL pepstatin A, 1 μg/mL aprotinin, 1 mM benzamadine, 2 mM phenylmethylsulfonyl fluoride) and processed for SDS-PAGE and immunoblotting.

For cytokine signaling assays *in vitro* generated rested effector T cells (5×10^5) were stimulated with IL-2 (1 ng/mL), IL-7 (1 ng/mL), or IL-15 (1 ng/mL) in 100 μL of RPMI 1640 supplemented with 1% (vol/vol) heat-inactivated FBS for the indicated times at 37°C. Cells were processed for intracellular staining with α-p(Y694)-STAT-5 and analyzed by flow cytometry.

Cell proliferation. For analyzing T cell proliferation by CellTrace Violet (CTV; Molecular Probes, Thermo Fisher Scientific) dilution, *in vitro* generated rested effector T cells (2×10^6) were incubated with CTV in d-PBS supplemented with 0.1% (vol/vol) bovine serum albumin (BSA) at a final concentration of 2 μM for 10 min at 37°C. Cells were then washed three times with d-PBS supplemented with 10% (vol/vol) FBS. T cells (3×10^5) in complete T cell medium (RPMI 1640 [Gibco/Life Technologies] supplemented with 10% [vol/vol] heat-inactivated FBS, 2 mM L-glutamine, 0.1 mM MEM nonessential amino acids, 1 mM sodium pyruvate, 10 mM HEPES, 100 U/mL penicillin, 100 μg/mL streptomycin, and 50 μM β-mercaptoethanol) were incubated with plate-bound α-mouse CD3ε (0 to 5 μg/mL) and α-mouse CD28 (2 μg/mL) for 2 to 4 days at 37°C. T cells were harvested, and the CTV dilution was analyzed by flow cytometry. Flow-count Fluorospheres (Beckman Coulter) were added to samples for cell quantification.

Generation of murine CAR T cells. Single cell suspensions were generated by mechanically disrupting spleens through a 40 μm cell strainer (Pall Corporation). Cells were washed once with PBS supplemented with 2% (vol/vol) FBS and then incubated in 1 mL of Red Blood Cell Lysing Buffer Hybri-Max (Sigma-Aldrich) for 5 min at room temperature to lyse red blood cells. Complete T cell medium was added to neutralize the red cell lysis buffer and cells pelleted ($300 \times g$, 5 min). Cells (2.5×10^7) were resuspended in 5 mL of complete T cell medium supplemented with α-CD3ε (0.5 μg/mL), α-CD28 (0.5 μg/mL), 10 ng/mL IL-2, and 0.2 ng/mL IL-7, followed by incubation in 6-well plates (Greiner BioOne) at 37°C and 5% CO_2 overnight. The next day, cells were harvested into 50-mL Falcon tubes (Corning) and resuspended in 20 mL of complete T cell medium. Dead cells were removed by underlaying 10 mL of Ficoll (GE Healthcare), followed by 20 min of centrifugation at 1,400 rpm at room temperature. Cells were harvested and washed twice with complete T cell medium before retroviral transduction. Retroviruses encoding a second-generation murine CAR consisting of an extracellular scFv-α-human HER2, a membrane-proximal CD8 hinge region, and the transmembrane and cytoplasmic signaling domains of CD28 fused to the cytoplasmic region of CD3ζ (scFv-α-HER2-CD28ζ) were obtained from the supernatants of the viral packaging GP+e86 cell line as described previously (37). 4-mL of retrovirus containing medium was added to RetroNectin-coated (10 μg/mL; TaKaRa Bio) nontreated 6-well plates (Corning Costar) and spun for 30 min ($1,200 \times g$) at room temperature. T cells (5×10^6 to 10×10^6) were resuspended in 1 mL of retroviral supernatant containing IL-2 (50 ng/mL) and IL-7 (1 ng/mL) and added to the RetroNectin- and virus-coated plates. T cells were centrifuged at $1,200 \times g$ for 90 min, followed by incubation overnight at 37°C and 5% CO_2 before a second round of viral transduction. Transduced T cells were maintained in complete T cell medium supplemented with IL-2 (5 ng/mL) and IL-7 (0.2 ng/mL) for 3 to 5 days at 37°C and 5% CO_2.

Generation of human T cells and CAR T cells. Human peripheral blood mononuclear cells (PBMCs) were isolated from healthy donor buffy coats. Human ethics approval for the use of PBMCs was granted by both the Australian Red Cross Blood Services and the Peter MacCallum Cancer Centre Human Research and Ethics committee (HREC 01/14), and the studies were conducted in accordance with the Australian Code for the Responsible Conduct of Research and the National Statement on Ethical Conduct in Human Research (National Health and Medical Research Council Act 1992). PBMCs (1×10^7 to 1.5×10^7) were activated with α-human CD3ε (OKT3; 30 ng/ml; eBioscience) in 10 mL of complete T cell medium (without β-mercaptoethanol) supplemented with IL-2 (20 ng/mL) for 2 to 3 days at 37°C and 5% CO_2. Human T cells were used for analyses after CRISPR/Cas9 genome editing or the generation of CAR T cells. For CAR T cell studies, retroviruses encoding a second-generation CAR consisting of an extracellular scFv-α-human Lewis Y (LeY), a membrane-proximal CD8 hinge region, and the transmembrane and cytoplasmic signaling domains of CD28 fused to the cytoplasmic region of CD3ζ were

obtained from the supernatants of PG13 packaging cells, as described previously (65, 66). Retroviral supernatants (5 ml) were spun for 30 min (1,200 × *g*) at room temperature onto RetroNectin (TaKaRa Bio)-coated (10 μg/mL) nontreated 6-well plates (Corning Costar) and incubated for 4 h at 37°C. Supernatants were removed and 2.5 × 10^6 human T cells were incubated overnight in 5 mL of complete T cell medium (without β-mercaptoethanol) supplemented with human IL-2 (20 ng/mL) before the second viral transduction. Transduced T cells were transferred into 25-cm^2 flasks and maintained in 5 to 10 mL of complete T cell medium supplemented (without β-mercaptoethanol) with IL-2 (20 ng/mL) for 1 to 2 weeks before analysis. At day 7 after retroviral transduction, CAR expression was assessed by staining with PE-conjugated α-FLAG (DYKDDDDK) tag (BioLegend, USA).

CAR T cell cytotoxicity assays. For the *in vitro* assessment of murine CAR T cell cytotoxicity, antigen-expressing 24JK-HER2 cells and antigen-negative 24JK sarcoma cells were labeled with CellTrace Violet (CTV; Invitrogen; Molecular Probes) at concentrations of 5 μM (CTV^{bright}) and 0.5 μM (CTV^{dim}), respectively, in d-PBS supplemented with 0.1% (vol/vol) BSA for 15 min at 37°C. Sarcoma cells were then washed three times with d-PBS supplemented with 10% (vol/vol) FBS and mixed at a 1:1 ratio and a concentration of 1 × 10^6/ml. CAR T cells were added at ratios of 20:1, 10:1, 5:1, 2.5:1, 1.25:1, and 0.6:1 to 5 × 10^4 CTV-labeled 24JK-HER2 cells (CTV^{bright}) and 5 × 10^4 CTV labeled antigen-negative 24JK sarcoma cells (CTV^{dim}), followed by incubation for 4 h at 37°C in 200 μL of complete T cell medium. Antigen-specific target cell lysis was analyzed by flow cytometry assessing the ratio between viable antigen-expressing cells and antigen-negative cells calculated using the formula: 100 × [(ER × %CTV^{dim} cells) – %CTV^{bright} cells]/(ER × %CTV^{dim} cells).

For the *in vitro* assessment of human CAR T cell cytotoxicity, a total of 5 × 10^6 cells OVCAR3 cells were labeled with 100 μCi of ^{51}Cr for 1 h at 37°C and 5% CO_2. After 1 h of incubation, tumor cells were washed three times with serum-free RPMI media by centrifugation (480 × *g*, 3 min). Cells were resuspended in supplemented RPMI media and plated at a density of 10,000 cells/well in V-bottom 96-well plates. Effector T cells were added to the appropriate wells at T cell/tumor cell ratios of 0.5:1, 1:1, 2:1, 5:1, or 10:1. In each experiment, control wells containing only ^{51}Cr-labeled tumor cells alone and wells containing tumor cells with 100 μl of SDS were included to determine spontaneous and total ^{51}Cr release, respectively. The total volume of supplemented RPMI media in each well was made to 200 μl, and the plates were incubated for 4 h at 37°C and 5% CO_2. After incubation, plates were centrifuged at 400 × *g* for 5 min, and 100 μl of supernatant from each well was transferred to 1.2-mL tubes (Quality Scientific Plastics). Chromium release was measured using an automatic gamma counter Wallac Wizard 1470 (General Electricity Healthcare). The percentage of tumor cell lysis was calculated according to the following formula: [(sample counts per minute – spontaneous counts per minute)/(total counts per minute – spontaneous counts per minute)] × 100%.

CAR T cell cytokine production assays. For murine HER2 CAR T cell analyses, 6 × 10^5 murine HER2 CAR T cells were cocultured with 3 × 10^5 HER2-expressing 24JK sarcoma cells or 3 × 10^5 HER2-negative 24JK sarcoma cells in round-bottom 96-well plate for 1 h at 37°C in complete T cell medium. GolgiPlug (1:1,000 dilution; BD Biosciences, San Jose, CA) and GolgiStop (1:1,500 dilution; BD Biosciences) were added for 3 to 4 h before cells were processed for surface and intracellular staining for CD8, IFN-γ, and TNF. The proportions of $CD8^+$ IFN-γ^+ or TNF^+ CAR T cells were determined by flow cytometry.

For human LeY CAR T cell analyses, 3 × 10^5 LeY CAR T cells generated from human PBMCs were cocultured with 3 × 10^5 LeY-expressing OVCAR-3 cells or 3 × 10^5 LeY negative MDA-MB-435 cells in round-bottom 96-well plates for 1 h at 37°C in complete T cell medium. GolgiPlug and GolgiStop were added at a 1:1,000 ratio for 3 to 4 h before the cells were processed for surface and intracellular staining for CD8, IFN-γ, and TNF. The proportions of $CD8^+$ IFN-γ^+ or TNF^+ CAR T cells were determined by flow cytometry.

Tumor studies in $PTPN22^{\Delta/\Delta}$ mice. Age-matched $Ptpn22^{+/+}$ and $Ptpn22^{\Delta/\Delta}$ female mice were anaesthetized with ketamine (100 mg/kg) and xylazil (10 mg/kg) (Troy Laboratories) and injected orthotopically with 2 × 10^5 AT3-OVA mammary tumor cells resuspended in 20 μL of d-PBS into the fourth mammary fat pad. Tumor area was measured every 2 days by multiplying the maximum diameter by the diameter perpendicular to the maximum diameter. Mice were sacrificed when tumor area reached ≥200 mm^2.

Adoptive CAR T cell therapy. For CAR T cell therapy experiments, C57BL/6 human-HER2 TG female mice were anaesthetized with ketamine (100 mg/kg) and xylazil (10 mg/kg) (Troy Laboratories) and injected orthotopically with 2 × 10^5 E0771-HER2 mammary tumor cells resuspended in 20 μL of d-PBS into the fourth mammary fat pad. Tumors were allowed to grow for 5 to 7 days prior to preconditioning with 4 Gy total body radiation. On the same day, mice were administered an intravenous injection of 1 × 10^7 α-HER2 CAR T cells, followed by a second CAR T cell injection the following day; control mice received no cells. For CAR T cell transfers, mice also received five doses of intraperitoneal IL-2 (50,000 IU/injection per mouse), with the first dose given on the same day as the first T cell injection and daily over the next 4 days. Tumor area was measured every 2 days by multiplying the maximum diameter by the diameter perpendicular to the maximum diameter. Mice were sacrificed when the tumor area reached ≥200 mm^2.

Adoptive OT-I T cell therapy. For OT-I T cell therapy experiments, $Ly5.1^+$ female mice were anaesthetized with ketamine (100 mg/kg) and xylazil (10 mg/kg) (Troy Laboratories) and injected orthotopically with 5 × 10^5 AT3-OVA mammary tumor cells resuspended in 20 μL of d-PBS into the fourth mammary fat pad. Alternatively, $Ly5.1^+$ male mice were injected subcutaneously with 5 × 10^5 MC38-OVA tumor cells resuspended in 100 μl of d-PBS into the flank. Tumors were allowed to grow for 7 days, and mice were then administered an intravenous injection of 1 × 10^7 OT-I $CD8^+Ly5.2^+$ T cells; control mice received no cells. Tumor area was measured every 2 days by multiplying the maximum diameter by the diameter perpendicular to the maximum diameter. Mice were sacrificed when tumor area reached ≥200 mm^2.

Analysis of tumor-infiltrating lymphocytes. Tumor-bearing mice were sacrificed, tumors were weighed, and up to 200 mg of tissue was digested in 12-well plates using a cocktail of 1 mg/mL collagenase type IV (Worthington Biochemicals) and 0.02 mg/mL DNase (Sigma-Aldrich) in DMEM supplemented with 2%

(vol/vol) FBS. The digestion was performed in a rocking incubator at 180 rotations per min for 30 min at 37°C. Cells were passed through a 70-μm cell strainer (BD Biosciences) twice and processed for flow cytometry.

Quantitative real-time PCR. RNA was extracted with TRIzol reagent (catalog no. 15596018; Thermo Fisher Scientific), and RNA quality and quantity were determined using a NanoDrop 2000 (Thermo Fisher Scientific). mRNA was reverse transcribed using a high-capacity cDNA reverse transcription kit (Applied Biosystems) and processed for quantitative real-time PCR using TaqMan gene expression assays. *Ptpn22* probe (Mm00501231_g1; Applied Biosystems) and *Gapdh* probe (Mm99999915_g1; Applied Biosystems) from TaqMan gene expression assays were utilized with TaqMan Fast advanced master mix (Applied Biosystems) to perform quantitative PCR detecting *Ptpn22* and *Gapdh*. The relative gene expression ($\Delta\Delta C_T$) was determined by normalization to the housekeeping gene *Gapdh*.

CRISPR/Cas9 genome editing in murine OT-I T cells. Single splenocyte suspensions from OT-I transgenic C57BL/6 mice were generated by mechanically disrupting spleens through a 45-μm cell strainer (Pall Corporation). Cells were washed once with PBS supplemented with 2% (vol/vol) FBS before incubation in 1 mL of Red Blood Cell Lysing Buffer Hybri-Max (Sigma-Aldrich) for 5 min at room temperature per spleen to lyse the red blood cells. Complete T cell medium was added to neutralize the red cell lysis buffer. To edit OT-I cells, 300 pmol of *Ptpn22* sgRNA (UUUGUCGGCCUUGUACUUGG; Synthego) or nontargeting control sgRNA (GCACUACCAGAGCUAACUCA; Synthego) and 37 pmol of recombinant Cas9 (IDT) were mixed to form ribonucleoproteins (RNPs). A total of 1×10^7 splenocytes were resuspended in 20 μL of 4D-Nucleofector Solution (16.4 μL of primary cell nucleofector solution supplemented with 3.6 μL of supplement; P3 Primary Cell 4D-Nucleofector X kit S, V4XP-3032, Lonza), combined with RNP and electroporated using the 4D-Nucleofector X Unit (Lonza) and the predefined nucleofection condition "T cell, mouse, unstim." Prewarmed T cell medium was added to electroporated cells and allowed 10 min for recovery. After CRISPR editing, OT-I cells were activated in 25-cm^2 flasks containing 10 mL of prewarmed completed T cell medium supplemented with N4 peptide (1 nM), IL-2 (5 ng/mL), and IL-7 (0.2 ng/mL) for 7 days before analysis or adoptive transfer.

CRISPR/Cas9 genome editing in human T cells and CAR T cells. Human T cells or CAR T cells were generated as described above and maintained in complete T cell medium (minus β-mercaptoethanol) supplemented with IL-2 (20 ng/mL) for 3 days before CRISPR RNP editing. To prepare complexes of Cas9/sgRNA RNP, 300 pmol of sgRNA targeting *PTPN22* (AAGGCAAUCUACCAAGUACA) or nontargeting control sgRNA (GCACUACCAGAGCUAACUCA) (Synthego) were premixed with 37 pmol of recombinant Cas9 (Alt-R S.p. Cas9 Nuclease V3; IDT) and incubated at room temperature for at least 10 min. 5×10^6 human T cells or CAR T cells were twice washed with 2% (vol/vol) FBS (in PBS) and resuspended in 20 μL of 4D-Nucleofector Solution (Lonza), followed by mixing with RNPs and incubation for 2 min at room temperature. Human T cells or CAR T cells were transferred into the retainer of 4D-Nucleofector X Unit (Lonza) and electroporated using predefined nucleofection condition "T cell, human, stim." Then, 200 μL of prewarmed complete T cell medium (minus β-mercaptoethanol) supplemented with IL-2 (20 ng/mL) was added to each well of the Nucleocuvette Strip, and electroporated cells were allowed to recover at 37°C and 5% CO_2 for 10 min before being transferred to 25-cm^2 flasks with 5 mL of prewarmed complete T cell medium (minus β-mercaptoethanol), supplemented with IL-2 (20 ng/mL), and cultured at 37°C and 5% CO_2 for 2 to 3 days before analysis.

Statistical analyses. All statistical analyses were performed with Prism software 7.0b (GraphPad, San Diego, CA) using the nonparametric using the two-tailed Mann-Whitney U test, the parametric two-tailed Student *t* test, or two-way analysis of variance (ANOVA), as indicated. Significance is indicated by asterisks in the figures (*, $P < 0.05$; **, $P < 0.01$; ***, $P < 0.001$; ****, $P < 0.0001$). The data are presented as means ± standard errors of the mean (SEM).

SUPPLEMENTAL MATERIAL

Supplemental material is available online only.

SUPPLEMENTAL FILE 1, PDF file, 3.6 MB.

ACKNOWLEDGMENTS

We thank Alexander Ziegler and Rachel Xu for technical support.

The *Ptpn22*$^{\Delta/\Delta}$ mutant mice were produced by the Monash Genome Modification Platform, Monash University, a node of Phenomics Australia that is supported by the National Collaborative Research Infrastructure Strategy, the Super Science Initiative and the Collaborative Research Infrastructure Scheme. This study was supported by the National Health and Medical Research Council (NHMRC) of Australia (T.T. and F.W.).

REFERENCES

1. Robbins PF, Lu Y-C, El-Gamil M, Li YF, Gross C, Gartner J, Lin JC, Teer JK, Cliften P, Tycksen E, Samuels Y, Rosenberg SA. 2013. Mining exomic sequencing data to identify mutated antigens recognized by adoptively transferred tumor-reactive T cells. Nat Med 19:747–752. https://doi.org/10.1038/nm.3161.
2. Rooney MS, Shukla SA, Wu CJ, Getz G, Hacohen N. 2015. Molecular and genetic properties of tumors associated with local immune cytolytic activity. Cell 160:48–61. https://doi.org/10.1016/j.cell.2014.12.033.
3. Ribas A, Wolchok JD. 2018. Cancer immunotherapy using checkpoint blockade. Science 359:1350–1355. https://doi.org/10.1126/science.aar4060.
4. Pardoll DM. 2012. The blockade of immune checkpoints in cancer immunotherapy. Nat Rev Cancer 12:252–264. https://doi.org/10.1038/nrc3239.
5. Fesnak AD, June CH, Levine BL. 2016. Engineered T cells: the promise and challenges of cancer immunotherapy. Nat Rev Cancer 16:566–581. https://doi.org/10.1038/nrc.2016.97.

6. Sadelain M, Riviere I, Riddell S. 2017. Therapeutic T cell engineering. Nature 545:423–431. https://doi.org/10.1038/nature22395.
7. Chan JD, Lai J, Slaney CY, Kallies A, Beavis PA, Darcy PK. 2021. Cellular networks controlling T cell persistence in adoptive cell therapy. Nat Rev Immunol 21:769–784. https://doi.org/10.1038/s41577-021-00539-6.
8. Davenport AJ, Cross RS, Watson KA, Liao Y, Shi W, Prince HM, Beavis PA, Trapani JA, Kershaw MH, Ritchie DS, Darcy PK, Neeson PJ, Jenkins MR. 2018. Chimeric antigen receptor T cells form nonclassical and potent immune synapses driving rapid cytotoxicity. Proc Natl Acad Sci U S A 115:E2068–E2076. https://doi.org/10.1073/pnas.1716266115.
9. Yong CSM, Dardalhon V, Devaud C, Taylor N, Darcy PK, Kershaw MH. 2017. CAR T-cell therapy of solid tumors. Immunol Cell Biol 95:356–363. https://doi.org/10.1038/icb.2016.128.
10. Maude SL, Frey N, Shaw PA, Aplenc R, Barrett DM, Bunin NJ, Chew A, Gonzalez VE, Zheng Z, Lacey SF, Mahnke YD, Melenhorst JJ, Rheingold SR, Shen A, Teachey DT, Levine BL, June CH, Porter DL, Grupp SA. 2014. Chimeric antigen receptor T cells for sustained remissions in leukemia. N Engl J Med 371:1507–1517. https://doi.org/10.1056/NEJMoa1407222.
11. Grupp SA, Kalos M, Barrett D, Aplenc R, Porter DL, Rheingold SR, Teachey DT, Chew A, Hauck B, Wright JF, Milone MC, Levine BL, June CH. 2013. Chimeric antigen receptor-modified T cells for acute lymphoid leukemia. N Engl J Med 368:1509–1518. https://doi.org/10.1056/NEJMoa1215134.
12. Wiede F, Lu K-H, Du X, Liang S, Hochheiser K, Dodd GT, Goh PK, Kearney C, Meyran D, Beavis PA, Henderson MA, Park SL, Waithman J, Zhang S, Zhang Z-Y, Oliaro J, Gebhardt T, Darcy PK, Tiganis T. 2020. PTPN2 phosphatase deletion in T cells promotes anti-tumor immunity and CAR T-cell efficacy in solid tumors. EMBO J 39:e103637. https://doi.org/10.15252/embj.2019103637.
13. Nishimura H, Nose M, Hiai H, Minato N, Honjo T. 1999. Development of lupus-like autoimmune diseases by disruption of the PD-1 gene encoding an ITIM motif-carrying immunoreceptor. Immunity 11:141–151. https://doi.org/10.1016/S1074-7613(00)80089-8.
14. Nishimura H, Okazaki T, Tanaka Y, Nakatani K, Hara M, Matsumori A, Sasayama S, Mizoguchi A, Hiai H, Minato N, Honjo T. 2001. Autoimmune dilated cardiomyopathy in PD-1 receptor-deficient mice. Science 291:319–322. https://doi.org/10.1126/science.291.5502.319.
15. Wang J, Yoshida T, Nakaki F, Hiai H, Okazaki T, Honjo T. 2005. Establishment of NOD-Pdcd1$^{-/-}$ mice as an efficient animal model of type I diabetes. Proc Natl Acad Sci U S A 102:11823–11828. https://doi.org/10.1073/pnas.0505497102.
16. Wiede F, Shields BJ, Chew SH, Kyparissoudis K, van Vliet C, Galic S, Tremblay ML, Russell SM, Godfrey DI, Tiganis T. 2011. T cell protein tyrosine phosphatase attenuates T cell signaling to maintain tolerance in mice. J Clin Invest 121:4758–4774. https://doi.org/10.1172/JCI59492.
17. Wiede F, La Gruta NL, Tiganis T. 2014. PTPN2 attenuates T-cell lymphopenia-induced proliferation. Nat Commun 5:3073. https://doi.org/10.1038/ncomms4073.
18. Wiede F, Sacirbegovic F, Leong YA, Yu D, Tiganis T. 2017. PTPN2-deficiency exacerbates T follicular helper cell and B cell responses and promotes the development of autoimmunity. J Autoimmun 76:85–100. https://doi.org/10.1016/j.jaut.2016.09.004.
19. Long SA, Cerosaletti K, Wan JY, Ho J-C, Tatum M, Wei S, Shilling HG, Buckner JH. 2011. An autoimmune-associated variant in PTPN2 reveals an impairment of IL-2R signaling in CD4$^+$ T cells. Genes Immun 12:116–125. https://doi.org/10.1038/gene.2010.54.
20. Wellcome Trust Case Control Consortium. 2007. Genome-wide association study of 14,000 cases of seven common diseases and 3,000 shared controls. Nature 447:661–678. https://doi.org/10.1038/nature05911.
21. Stanford SM, Bottini N. 2014. PTPN22: the archetypal non-HLA autoimmunity gene. Nat Rev Rheumatol 10:602–611. https://doi.org/10.1038/nrrheum.2014.109.
22. Bottini N, Peterson EJ. 2014. Tyrosine phosphatase PTPN22: multifunctional regulator of immune signaling, development, and disease. Annu Rev Immunol 32:83–119. https://doi.org/10.1146/annurev-immunol-032713-120249.
23. Hasegawa K, Martin F, Huang G, Tumas D, Diehl L, Chan AC. 2004. PEST domain-enriched tyrosine phosphatase (PEP) regulation of effector/memory T cells. Science 303:685–689. https://doi.org/10.1126/science.1092138.
24. Maine CJ, Hamilton-Williams EE, Cheung J, Stanford SM, Bottini N, Wicker LS, Sherman LA. 2012. PTPN22 alters the development of regulatory T cells in the thymus. J Immunol 188:5267–5275. https://doi.org/10.4049/jimmunol.1200150.
25. Brownlie RJ, Miosge LA, Vassilakos D, Svensson LM, Cope A, Zamoyska R. 2012. Lack of the phosphatase PTPN22 increases adhesion of murine regulatory T cells to improve their immunosuppressive function. Sci Signal 5:ra87. https://doi.org/10.1126/scisignal.2003365.
26. Wang Y, Shaked I, Stanford SM, Zhou W, Curtsinger JM, Mikulski Z, Shaheen ZR, Cheng G, Sawatzke K, Campbell AM, Auger JL, Bilgic H, Shoyama FM, Schmeling DO, Balfour HH, Hasegawa K, Chan AC, Corbett JA, Binstadt BA, Mescher MF, Ley K, Bottini N, Peterson EJ. 2013. The autoimmunity-associated gene PTPN22 potentiates Toll-like receptor-driven, type 1 interferon-dependent immunity. Immunity 39:111–122. https://doi.org/10.1016/j.immuni.2013.06.013.
27. Spalinger MR, Kasper S, Gottier C, Lang S, Atrott K, Vavricka SR, Scharl S, Raselli T, Frey-Wagner I, Gutte PM, Grütter MG, Beer H-D, Contassot E, Chan AC, Dai X, Rawlings DJ, Mair F, Becher B, Falk W, Fried M, Rogler G, Scharl M. 2016. NLRP3 tyrosine phosphorylation is controlled by protein tyrosine phosphatase PTPN22. J Clin Invest 126:1783–1800. https://doi.org/10.1172/JCI83669.
28. Cubas R, Khan Z, Gong Q, Moskalenko M, Xiong H, Ou Q, Pai C, Rodriguez R, Cheung J, Chan AC. 2020. Autoimmunity linked protein phosphatase PTPN22 as a target for cancer immunotherapy. J Immunother Cancer 8:e001439. https://doi.org/10.1136/jitc-2020-001439.
29. Brownlie RJ, Wright D, Zamoyska R, Salmond RJ. 2019. Deletion of PTPN22 improves effector and memory CD8$^+$ T cell responses to tumors. JCI Insight 4:e127847. https://doi.org/10.1172/jci.insight.127847.
30. Brownlie RJ, Garcia C, Ravasz M, Zehn D, Salmond RJ, Zamoyska R. 2017. Resistance to TGFβ suppression and improved antitumor responses in CD8$^+$ T cells lacking PTPN22. Nat Commun 8:1343. https://doi.org/10.1038/s41467-017-01427-1.
31. Cong L, Ran FA, Cox D, Lin S, Barretto R, Habib N, Hsu PD, Wu X, Jiang W, Marraffini LA, Zhang F. 2013. Multiplex genome engineering using CRISPR/Cas systems. Science 339:819–823. https://doi.org/10.1126/science.1231143.
32. Stewart TJ, Abrams SI. 2007. Altered immune function during long-term host-tumor interactions can be modulated to retard autochthonous neoplastic growth. J Immunol 179:2851–2859. https://doi.org/10.4049/jimmunol.179.5.2851.
33. Mattarollo SR, Loi S, Duret H, Ma Y, Zitvogel L, Smyth MJ. 2011. Pivotal role of innate and adaptive immunity in anthracycline chemotherapy of established tumors. Cancer Res 71:4809–4820. https://doi.org/10.1158/0008-5472.CAN-11-0753.
34. Stadtmauer EA, Fraietta JA, Davis MM, Cohen AD, Weber KL, Lancaster E, Mangan PA, Kulikovskaya I, Gupta M, Chen F, Tian L, Gonzalez VE, Xu J, Jung I-y, Melenhorst JJ, Plesa G, Shea J, Matlawski T, Cervini A, Gaymon AL, Desjardins S, Lamontagne A, Salas-Mckee J, Fesnak A, Siegel DL, Levine BL, Jadlowsky JK, Young RM, Chew A, Hwang W-T, Hexner EO, Carreno BM, Nobles CL, Bushman FD, Parker KR, Qi Y, Satpathy AT, Chang HY, Zhao Y, Lacey SF, June CH. 2020. CRISPR-engineered T cells in patients with refractory cancer. Science 367:eaba7365. https://doi.org/10.1126/science.aba7365.
35. Kim S, Kim D, Cho SW, Kim J, Kim JS. 2014. Highly efficient RNA-guided genome editing in human cells via delivery of purified Cas9 ribonucleoproteins. Genome Res 24:1012–1019. https://doi.org/10.1101/gr.171322.113.
36. Lin S, Staahl BT, Alla RK, Doudna JA. 2014. Enhanced homology-directed human genome engineering by controlled timing of CRISPR/Cas9 delivery. Elife 3:e04766. https://doi.org/10.7554/eLife.04766.
37. Haynes NM, Trapani JA, Teng MWL, Jackson JT, Cerruti L, Jane SM, Kershaw MH, Smyth MJ, Darcy PK. 2002. Single-chain antigen recognition receptors that costimulate potent rejection of established experimental tumors. Blood 100:3155–3163. https://doi.org/10.1182/blood-2002-04-1041.
38. Mardiana S, John LB, Henderson MA, Slaney CY, von Scheidt B, Giuffrida L, Davenport AJ, Trapani JA, Neeson PJ, Loi S, Haynes NM, Kershaw MH, Beavis PA, Darcy PK. 2017. A multifunctional role for adjuvant anti-4-1BB therapy in augmenting anti-tumor response by chimeric antigen receptor T cells. Cancer Res 77:1296–1309. https://doi.org/10.1158/0008-5472.CAN-16-1831.
39. Piechocki MP, Ho YS, Pilon S, Wei WZ. 2003. Human ErbB-2 (Her-2) transgenic mice: a model system for testing Her-2 based vaccines. J Immunol 171:5787–5794. https://doi.org/10.4049/jimmunol.171.11.5787.
40. Sommermeyer D, Hudecek M, Kosasih PL, Gogishvili T, Maloney DG, Turtle CJ, Riddell SR. 2016. Chimeric antigen receptor-modified T cells derived from defined CD8$^+$ and CD4$^+$ subsets confer superior antitumor reactivity *in vivo*. Leukemia 30:492–500. https://doi.org/10.1038/leu.2015.247.
41. Moeller M, Haynes NM, Kershaw MH, Jackson JT, Teng MWL, Street SE, Cerutti L, Jane SM, Trapani JA, Smyth MJ, Darcy PK. 2005. Adoptive transfer of gene-engineered CD4$^+$ helper T cells induces potent primary and secondary tumor rejection. Blood 106:2995–3003. https://doi.org/10.1182/blood-2004-12-4906.
42. Ahrends T, Spanjaard A, Pilzecker B, Bąbała N, Bovens A, Xiao Y, Jacobs H, Borst J. 2017. CD4$^+$ T cell help confers a cytotoxic T cell effector program

including coinhibitory receptor downregulation and increased tissue invasiveness. Immunity 47:848–861. https://doi.org/10.1016/j.immuni.2017.10.009.
43. Alspach E, Lussier DM, Miceli AP, Kizhvatov I, DuPage M, Luoma AM, Meng W, Lichti CF, Esaulova E, Vomund AN, Runci D, Ward JP, Gubin MM, Medrano RFV, Arthur CD, White JM, Sheehan KCF, Chen A, Wucherpfennig KW, Jacks T, Unanue ER, Artyomov MN, Schreiber RD. 2019. MHC-II neoantigens shape tumor immunity and response to immunotherapy. Nature 574:696–701. https://doi.org/10.1038/s41586-019-1671-8.
44. Ritchie DS, Neeson PJ, Khot A, Peinert S, Tai T, Tainton K, Chen K, Shin M, Wall DM, Hönemann D, Gambell P, Westerman DA, Haurat J, Westwood JA, Scott AM, Kravets L, Dickinson M, Trapani JA, Smyth MJ, Darcy PK, Kershaw MH, Prince HM. 2013. Persistence and efficacy of second generation CAR T cell against the LeY antigen in acute myeloid leukemia. Mol Ther 21:2122–2129. https://doi.org/10.1038/mt.2013.154.
45. Westwood JA, Smyth MJ, Teng MWL, Moeller M, Trapani JA, Scott AM, Smyth FE, Cartwright GA, Power BE, Hönemann D, Prince HM, Darcy PK, Kershaw MH. 2005. Adoptive transfer of T cells modified with a humanized chimeric receptor gene inhibits growth of Lewis-Y-expressing tumors in mice. Proc Natl Acad Sci U S A 102:19051–19056. https://doi.org/10.1073/pnas.0504312102.
46. Giuffrida L, Sek K, Henderson MA, Lai J, Chen AXY, Meyran D, Todd KL, Petley EV, Mardiana S, Mølck C, Stewart GD, Solomon BJ, Parish IA, Neeson PJ, Harrison SJ, Kats LM, House IG, Darcy PK, Beavis PA. 2021. CRISPR/Cas9 mediated deletion of the adenosine A2A receptor enhances CAR T cell efficacy. Nat Commun 12:3236. https://doi.org/10.1038/s41467-021-23331-5.
47. Scott AC, Dündar F, Zumbo P, Chandran SS, Klebanoff CA, Shakiba M, Trivedi P, Menocal L, Appleby H, Camara S, Zamarin D, Walther T, Snyder A, Femia MR, Comen EA, Wen HY, Hellmann MD, Anandasabapathy N, Liu Y, Altorki NK, Lauer P, Levy O, Glickman MS, Kaye J, Betel D, Philip M, Schietinger A. 2019. TOX is a critical regulator of tumor-specific T cell differentiation. Nature 571:270–274. https://doi.org/10.1038/s41586-019-1324-y.
48. Seo H, Chen J, González-Avalos E, Samaniego-Castruita D, Das A, Wang YH, López-Moyado IF, Georges RO, Zhang W, Onodera A, Wu C-J, Lu L-F, Hogan PG, Bhandoola A, Rao A. 2019. TOX and TOX2 transcription factors cooperate with NR4A transcription factors to impose $CD8^+$ T cell exhaustion. Proc Natl Acad Sci U S A 116:12410–12415. https://doi.org/10.1073/pnas.1905675116.
49. Lu Y, Xue J, Deng T, Zhou X, Yu K, Deng L, Huang M, Yi X, Liang M, Wang Y, Shen H, Tong R, Wang W, Li L, Song J, Li J, Su X, Ding Z, Gong Y, Zhu J, Wang Y, Zou B, Zhang Y, Li Y, Zhou L, Liu Y, Yu M, Wang Y, Zhang X, Yin L, Xia X, Zeng Y, Zhou Q, Ying B, Chen C, Wei Y, Li W, Mok T. 2020. Safety and feasibility of CRISPR-edited T cells in patients with refractory non-small-cell lung cancer. Nat Med 26:732–740. https://doi.org/10.1038/s41591-020-0840-5.
50. Ho WJ, Croessmann S, Lin J, Phyo ZH, Charmsaz S, Danilova L, et al. 2021. Systemic inhibition of PTPN22 augments anticancer immunity. J Clin Invest 131:e146950. https://doi.org/10.1172/JCI146950.
51. Hogquist KA, Baldwin TA, Jameson SC. 2005. Central tolerance: learning self-control in the thymus. Nat Rev Immunol 5:772–782. https://doi.org/10.1038/nri1707.
52. Yarchoan M, Johnson BA, III, Lutz ER, Laheru DA, Jaffee EM. 2017. Targeting neoantigens to augment antitumour immunity. Nat Rev Cancer 17:209–222. https://doi.org/10.1038/nrc.2016.154.
53. Schumacher TN, Schreiber RD. 2015. Neoantigens in cancer immunotherapy. Science 348:69–74. https://doi.org/10.1126/science.aaa4971.
54. Kalos M, June CH. 2013. Adoptive T cell transfer for cancer immunotherapy in the era of synthetic biology. Immunity 39:49–60. https://doi.org/10.1016/j.immuni.2013.07.002.
55. Braendstrup P, Levine BL, Ruella M. 2020. The long road to the first FDA-approved gene therapy: chimeric antigen receptor T cells targeting CD19. Cytotherapy 22:57–69. https://doi.org/10.1016/j.jcyt.2019.12.004.
56. LaFleur MW, Nguyen TH, Coxe MA, Miller BC, Yates KB, Gillis JE, Sen DR, Gaudiano EF, Al Abosy R, Freeman GJ, Haining WN, Sharpe AH. 2019. PTPN2 regulates the generation of exhausted $CD8^+$ T cell subpopulations and restrains tumor immunity. Nat Immunol 20:1335–1347. https://doi.org/10.1038/s41590-019-0480-4.
57. Holmes DA, Suto E, Lee WP, Ou Q, Gong Q, Smith HRC, Caplazi P, Chan AC. 2015. Autoimmunity-associated protein tyrosine phosphatase PEP negatively regulates IFN-α receptor signaling. J Exp Med 212:1081–1093. https://doi.org/10.1084/jem.20142130.
58. Salmond RJ, Brownlie RJ, Morrison VL, Zamoyska R. 2014. The tyrosine phosphatase PTPN22 discriminates weak self peptides from strong agonist TCR signals. Nat Immunol 15:875–883. https://doi.org/10.1038/ni.2958.
59. Wiede F, Lu K-H, Du X, Zeissig MN, Xu R, Goh PK, Xirouchaki CE, Hogarth SJ, Greatorex S, Sek K, Daly RJ, Beavis PA, Darcy PK, Tonks NK, Tiganis T. 2021. PTP1B is an intracellular checkpoint that limits T cell and CAR T cell anti-tumor immunity. Cancer Discov. https://doi.org/10.1158/2159-8290.CD-21-0694.
60. Wiede F, Ziegler A, Zehn D, Tiganis T. 2014. PTPN2 restrains $CD8^+$ T cell responses after antigen cross-presentation for the maintenance of peripheral tolerance in mice. J Autoimmun 53:105–114. https://doi.org/10.1016/j.jaut.2014.05.008.
61. Wiede F, Brodnicki TC, Goh PK, Leong YA, Jones GW, Yu D, Baxter AG, Jones SA, Kay TWH, Tiganis T. 2019. T-cell-specific PTPN2 deficiency in NOD mice accelerates the development of type 1 diabetes and autoimmune comorbidities. Diabetes 68:1251–1266. https://doi.org/10.2337/db18-1362.
62. Johnstone CN, Smith YE, Cao Y, Burrows AD, Cross RSN, Ling X, Redvers RP, Doherty JP, Eckhardt BL, Natoli AL, Restall CM, Lucas E, Pearson HB, Deb S, Britt KL, Rizzitelli A, Li J, Harmey JH, Pouliot N, Anderson RL. 2015. Functional and molecular characterization of EO771.LMB tumors, a new C57BL/6-mouse-derived model of spontaneously metastatic mammary cancer. Dis Model Mech 8:237–251. https://doi.org/10.1242/dmm.017830.
63. Shiloni E, Karp SE, Custer MC, Shilyansky J, Restifo NP, Rosenberg SA, Mulé JJ. 1993. Retroviral transduction of interferon-gamma cDNA into a nonimmunogenic murine fibrosarcoma: generation of T cells in draining lymph nodes capable of treating established parental metastatic tumor. Cancer Immunol Immunother 37:286–292. https://doi.org/10.1007/BF01518450.
64. Kershaw MH, Jackson JT, Haynes NM, Teng MWL, Moeller M, Hayakawa Y, Street SE, Cameron R, Tanner JE, Trapani JA, Smyth MJ, Darcy PK. 2004. Gene-engineered T cells as a superior adjuvant therapy for metastatic cancer. J Immunol 173:2143–2150. https://doi.org/10.4049/jimmunol.173.3.2143.
65. Westwood JA, Murray WK, Trivett M, Shin A, Neeson P, MacGregor DP, Haynes NM, Trapani JA, Mayura-Guru P, Fox S, Peinert S, Honemann D, Prince HM, Ritchie D, Scott AM, Smyth FE, Smyth MJ, Darcy PK, Kershaw MH. 2008. Absence of retroviral vector-mediated transformation of gene-modified T cells after long-term engraftment in mice. Gene Ther 15:1056–1066. https://doi.org/10.1038/gt.2008.47.
66. Peinert S, Prince HM, Guru PM, Kershaw MH, Smyth MJ, Trapani JA, Gambell P, Harrison S, Scott AM, Smyth FE, Darcy PK, Tainton K, Neeson P, Ritchie DS, Hönemann D. 2010. Gene-modified T cells as immunotherapy for multiple myeloma and acute myeloid leukemia expressing the Lewis Y antigen. Gene Ther 17:678–686. https://doi.org/10.1038/gt.2010.21.